

DUPLICATE ALSO

NATIONAL
METEOROLOGICAL

LIBRARY

OCEAN APPLICATIONS TECHNICAL NOTE 4.

**SIMULATIONS OF THE OCEAN CARBON CYCLE FOR THE PERIOD 1765 TO
1990 AND BEYOND IN A SEASONALLY FORCED OCEAN GENERAL
CIRCULATION MODEL**

by

N. K. TAYLOR

Met Office

FitzRoy Road, Exeter, Devon. EX1 3PB

© Crown Copyright 1995

**This document has not been published. Permission to quote from it must be obtained
from the Head of Ocean Applications at the above address.**

SIMULATIONS OF THE OCEAN CARBON CYCLE FOR THE PERIOD 1765 TO 1990 AND BEYOND IN A SEASONALLY FORCED OCEAN GENERAL CIRCULATION MODEL

N. K. Taylor

Hadley Centre for Climate Prediction and Research

Meteorological Office

Bracknell, UK

ABSTRACT

This paper describes the Hadley Centre ocean carbon cycle model, which is based on the Hadley Centre 3-D general circulation model with the addition of tracer and carbon cycle components. The model has been used to simulate the pre-industrial carbon cycle and to estimate the uptake of transient tracers from 1765 to 1990. The model's average uptake of carbon dioxide (CO₂) for the period 1980-89 is 2.0 GtC yr⁻¹, which lies at the centre of the range of current IPCC estimates. However, much of this occurs in the Southern hemisphere, and comparison of modelled uptake of excess CO₂, bomb radiocarbon and CFC-11 all suggest that the penetration of transient tracers in the high southern latitudes is too strong. Elsewhere, model predictions are supported by the observations. The model is also used to estimate the future levels of CO₂ emissions required to achieve given atmospheric CO₂ concentration targets of 450 ppm (1.6 times pre-industrial) and 650 ppm (2.3 times pre-industrial). In both cases, the ultimate level of emissions is required to be substantially lower than at present if atmospheric concentrations are to be stabilised.

1 INTRODUCTION

In recent years there has been a great deal of interest in the role of the so-called greenhouse gases in climate and the possibility of climate change brought about by man's activities in significantly increasing their atmospheric concentration. A related area that has also attracted a lot of attention is that of the carbon cycle. The reason for this is that since CO₂ is the dominant greenhouse gas, the past, present and future movements of carbon between its various source and sinks needs to be known in some detail if we are to understand present-day and past levels of greenhouse gas concentrations in the atmosphere and if we are to be able to predict the course of climate change into the future.

Predictions of climate change are often made using global climate models consisting of an atmospheric general circulation model (or GCM) coupled to an ocean GCM. These predictions then depend upon knowing what the future amount of CO₂ and other trace gases will be in the atmosphere. One way to estimate future levels of CO₂ is to use a carbon cycle model which is forced with estimated scenarios for future industrial CO₂ emissions. A popular method of achieving this aim has been to use simplified geochemical box models, such as those of Oeschger *et al* (1975) and Siegenthaler (1983). More recently, with the advent of faster and more powerful supercomputers, ocean carbon cycle models based upon GCMs have been developed (Maier-Reimer and Hasselmann, 1987; Sarmiento *et al*, 1992; Taylor, 1995; Orr and Monfray, *in prep*). These 3-D models are based on more complete physics than the box models and have the potential to be used for investigations of the effect of feedback mechanisms on CO₂ uptake and transport. Moreover, if they are run coupled to an atmospheric GCM, the coupled model is able to take account of these feedbacks and can compute the future concentration of CO₂ in the atmosphere as a response to climate change.

This paper describes the Hadley Centre ocean carbon cycle model and presents a comparison of simulated CO₂ and bomb radiocarbon uptake rates against observations for the period 1765-1990. The model is used to investigate the response to two different scenarios of future atmospheric CO₂ growth, and an assessment made of the required industrial emissions needed to attain these targets. Apart from bomb radiocarbon, tritium and CFCs -11 and -12 were also used to validate the model. These other tracers are of particular use for examining aspects of model behaviour not well-covered by bomb ¹⁴C. Uptake of CFC-11 in the Southern Ocean will be briefly considered here, although a full discussion of the simulations of these tracers is the subject of a separate article (Taylor, 1995, *in prep*).

The ocean and carbon cycle components of the model are described in Section 2, steady-state pre-industrial tracer distributions are presented in Section 3.1, and industrial CO₂ uptake simulations are discussed in Section 3.2. Section 3.3 looks at the emission scenarios required to satisfy future CO₂ targets, bomb radiocarbon uptake simulations are discussed in Section 3.4 and in Sections 3.5 and 3.6 we consider the effect that parametrisations of the Mediterranean outflow and isopycnal mixing have on the model results. Conclusions follow in Section 4.

2 MODEL DESCRIPTION

The model consists of two separate components: an ocean GCM which is the same model used for climate change modelling at the Hadley Centre, and an inorganic ocean carbon cycle model which is embedded within the GCM.

2.1 Ocean Circulation Model

The ocean circulation model used is based upon the 3-D primitive equation model described by Bryan (1969) and Cox (1984), which solves the Navier-Stokes equations modified by the Boussinesq approximation and hydrostatic assumption. Prognostic variables are temperature, salinity, and zonal and meridional velocity. Density is computed from temperature and salinity using a polynomial approximation to the equation of state for seawater (Bryan and Cox, 1972) and vertical velocity is diagnosed from the continuity equation. A detailed description of the equations and their method of solution can be found in the above references. The model employed here is global and includes a realistic approximation to bottom topography and continental coastlines. A horizontal grid resolution of 2.5° latitude by 3.75° longitude was chosen to match the resolution of the Hadley Centre atmospheric climate model (Murphy and Mitchell, 1995). 20 levels are used in the vertical with 7 levels covering the top 113 metres (Table 1). The near-surface resolution is somewhat higher than other models of this type, since it is recognized that a good representation of vertical mixing processes near to the surface is important for modelling the seasonal exchange of CO₂ with the atmosphere. A Kraus-Turner type bulk mixed layer model (Kraus and Turner, 1967) is incorporated within the ocean model in order to improve the simulation of the seasonal cycle of sea surface temperature and mixed layer depths (Sterl and Kattenberg, 1994). In the version of the model used here, SST is not permitted to drift far away from observations (see below), but in versions that are coupled to an atmospheric GCM it is important to reduce errors in simulating seasonal changes in SST. Energy provided by wind mixing power is used to mix the surface heat and freshwater input throughout the mixed layer. Wind-mixing energy is decayed exponentially with depth to prevent over-deepening of the winter-time mixed layer. Convection in the mixed layer is partly penetrative in that 85% of convectively generated turbulent kinetic energy is dissipated within the mixed layer. Penetrative short wave radiation is represented by a double exponential decay function (Paulson and Simpson, 1977). As well as the Kraus-Turner scheme, we use the K-theory mixing scheme of Pacanowski and Philander (1981) to parametrize Richardson-Number-dependent vertical turbulent mixing. In this scheme the mixing coefficients are enhanced wherever stratification is low and vertical shear is high, but are not allowed to fall below minimum background values. The background vertical eddy viscosity is chosen as $0.1 \text{ cm}^2 \text{ s}^{-1}$, while the background value of the eddy diffusivity increases linearly from $0.1 \text{ cm}^2 \text{ s}^{-1}$ at the surface to $1.5 \text{ cm}^2 \text{ s}^{-1}$ below 1500m, according to the profile described by Kraus (1988). Below the thermocline the values used by the model are essentially the background ones.

Below the mixed layer the complete convection algorithm of Rahmsdorf (1993) is used. Unlike the standard Cox scheme for convective mixing, this new scheme guarantees complete static stability after one pass through the subroutine.

A parametrization of isopycnal diffusion (Redi, 1982 ; Cox, 1987) is included so that the dominant direction of mixing for tracers such as heat, salt and carbon lies along surfaces of constant density rather than the horizontal. It is believed that this more accurately mimics the thermocline ventilation and mixing processes that occur in the real ocean. England (1993) found that the inclusion of an isopycnal mixing scheme resulted in an improvement in the simulated production of intermediate water. Isopycnal diffusivity is assumed to be greater in the upper ocean than in the deep ocean:

$$A_b = A_s + (A_s - A_b) \exp(-z/500) \quad (1)$$

where A_s is the surface value, A_b is the deep ocean value, and z is the depth in metres. We use $A_b = 0.4 \times 10^3 \text{ m}^2 \text{ s}^{-1}$, $A_s = 2.0 \times 10^3 \text{ m}^2 \text{ s}^{-1}$. We include a modification to the scheme due to Gerdes *et al* (1991), which reduces the amount of implied diapycnal diffusivity in situations where the slope of the isopycnals is large. To keep the isopycnal scheme stable, whenever the isopycnals exceed a maximum slope of 1 in 100, the vertical derivative of density is set to the value of the maximum slope. The modified scheme then scales the isopycnal diffusion according to the slope, so that there is less diffusion when the slope is large. In addition to the isopycnal component of diffusivity, a small background horizontal coefficient is included to maintain numerical stability. The isopycnal scheme is switched off over the top 50m to avoid a possible interaction between the isopycnal and mixed layer schemes which can cause a drift to occur when a switch is made from synchronous to asynchronous forcing (R. Wood, personal communication). In the top 50m, horizontal diffusion is used instead.

Because of the convergence of meridians at high latitudes, horizontal viscosity is decreased away from the equator according to:

$$A_m = A_{m1} + A_{m2} \cos \phi \quad (2)$$

where ϕ is latitude. In all runs, $A_{m1} = A_{m2} = 1.5 \times 10^5 \text{ m}^2 \text{ s}^{-1}$. The smaller coefficient of viscosity at the poles enables a longer timestep to be used without violating the grid cell Reynolds number stability criterion.

The coarse horizontal resolution means that the Straits of Gibraltar are not resolved by the model grid. However, the Mediterranean Sea is included in the model, and exchange through the straits of Gibraltar is parametrized in a simple way, using the method described by Manabe and Stouffer (1988). At each timestep the tracer properties of the Atlantic and Mediterranean grid points adjacent to the Straits are fully mixed down to a depth of 1200 metres. In this way a source of Mediterranean water is introduced into the Atlantic at the correct depth.

Because the model's surface temperature and salinity are forced towards climatology in these runs, there is no need to

include a full sea-ice model to correctly simulate water formation. However, ice cover has a large influence on gas exchange, and so a very simple parametrization of the effects of sea-ice is used. Areas of ocean where the climatological SST is equal to -1.8°C or less are deemed to be ice points and air-sea fluxes are switched off at these points.

The model is forced with Esbensen and Kushnir (1981) heat fluxes and the climatological wind stresses of Hellerman and Rosenstein (1983). Surface fresh water fluxes were obtained by combining the Jaeger (1976) precipitation dataset with evaporation derived from the Esbensen and Kushnir fluxes. In addition to the prescribed heat and salt fluxes, surface values of temperature and salinity are relaxed back towards climatological values using a method equivalent to that of Haney (1971), so that the surface boundary condition takes the form

$$Q(T) = Q(T_c) + \lambda (T - T_c) \quad (3)$$

$$F(S) = F(S_c) + \lambda (S - S_c)/C_p \quad (4)$$

where $Q(T_c)$, $F(S_c)$ are the climatological heat and salt fluxes for the climatological sea surface temperature (T_c) and sea surface salinity (S_c), and T, S are the surface values of temperature and salinity predicted by the model. T_c are derived from a joint UKMO/Massachusetts Institute of Technology dataset of SST (Bottomley *et al.*, 1990), and S_c are taken from Levitus (1982). C_p is the specific heat capacity of seawater in $\text{J Kg}^{-1} \text{K}^{-1}$. λ takes the value $40.9 \text{ Wm}^{-2} \text{K}^{-1}$, which corresponds to a relaxation timescale of about 60 days for a surface mixed layer of depth 50m. This formulation prevents the surface temperatures and salinities from drifting far away from climatology.

A well-known problem with the climatological forcing for salinity is that the salinities around the coast of Antarctica in the Levitus dataset are biased toward the summertime values, and are thus too fresh. This inhibits the formation of Antarctic Bottom Water (England, 1993; Taylor, 1995). We therefore increased the salinities used for the relaxation in equation (4) during austral summer in the Ross and Weddell seas as suggested by England (1993).

2.2 Carbon Cycle Model

The carbon cycle model is designed to be as simple as possible. The 3-dimensional distribution of dissolved inorganic carbon is calculated within the interior of the ocean model using

$$\partial C / \partial t + \underline{u} \cdot \nabla C + w \partial C / \partial z = A_h \nabla^2 C + \partial (K_h \partial C / \partial z) / \partial z \quad (5)$$

where C is the concentration of dissolved inorganic carbon. Except for at the surface, C is thus treated as an additional conservative tracer by the ocean circulation model. The same mixing coefficients are used for dissolved inorganic carbon and the other tracers as for temperature and salinity.

The equations given by Peng *et al.* (1987) and the computational procedure of Bacastow (1981) are used to compute the partial pressure of CO_2 at the sea surface. The Peng *et al.* (1987) equations use dissociation constants determined by

Mehrbach *et al* (1973). These have been superceded by the more recent measurements of Goyet and Poisson (1989) which are thought to be more accurate, but for the purposes of this paper the differences are very small. The flux of carbon dioxide between atmosphere and ocean is expressed as the product of a gas transfer coefficient and the partial pressure difference between air and water (Etcheto and Merlivat, 1988; Tans *et al*, 1990; Thomas *et al*, 1988):

$$\begin{aligned}\text{Flux} &= V_p k_0 (p\text{CO}_2^{(\text{atm})} - p\text{CO}_2^{(\text{oc})}) \\ &= V_p k_0 \Delta p\text{CO}_2\end{aligned}\quad (6)$$

where k_0 is the CO_2 solubility, $p\text{CO}_2^{(\text{atm})}$ and $p\text{CO}_2^{(\text{oc})}$ are the partial pressures in the atmosphere and the ocean, and V_p is a piston velocity. The product $V_p k_0$ is the gas transfer coefficient. $p\text{CO}_2^{(\text{atm})}$ is assumed to be spatially constant, so that the atmosphere is treated as a single well-mixed box.

In most of the runs the piston velocity, V_p , is computed from wind-speed according to Liss and Merlivat (1986):

$$\begin{aligned}V_p &= (S_c/600)^{-2/3} 0.17 U & U < 3.6 \text{ ms}^{-1} \\ V_p &= (S_c/600)^{-1/2} (2.85 U - 9.65) & 3.6 \leq U < 13.0 \text{ ms}^{-1} \\ V_p &= (S_c/600)^{-1/2} (5.9 U - 49.3) & 13.0 \text{ ms}^{-1} \leq U\end{aligned}\quad (7)$$

where S_c is the Schmidt number. The Schmidt number is a measure of the competing effects of gas diffusion and fluid viscosity on gas transfer and is calculated from the formula given by Wanninkhof (1992):

$$S_c = 2073.1 - 125.62 T + 3.6276 T^2 - 0.043219 T^3 \quad (8)$$

This formulation, when used with wind-speeds computed from the seasonally varying Hellerman windstresses, gives an annually-averaged global mean gas exchange rate of $0.045 \text{ moles } \mu\text{atm}^{-1} \text{ m}^{-2} \text{ yr}^{-1}$. To facilitate comparison with other models, we also repeated some of the runs using a spatially constant gas transfer coefficient of $0.067 \text{ moles } \mu\text{atm}^{-1} \text{ m}^{-2} \text{ yr}^{-1}$ determined from observations of bomb radiocarbon distribution (Broecker *et al*, 1985a).

The biological pump is not included in this version of the model, as the aim of these experiments is to examine the response of the model to anthropogenic increases in atmospheric CO_2 , for which the biological pump is assumed to act as a steady, unchanging background. As a result of this omission, the deep water TCO_2 is underestimated by about $250 \mu\text{mole kg}^{-1}$ and so absolute inventories of total carbon cannot be compared with observations. This particular version of the model is therefore only suitable for looking at perturbations to the inventory.

2.3 Inclusion Of Radiocarbon

^{14}C is included as a passive tracer in a similar manner to the procedure used by Toggweiler *et al* (1989a), using an arbitrary fixed atmospheric composition of 100 model units to represent the pre-industrial atmosphere and a half-life for

radioactive decay of 5730 years. Results are reported in the conventional units as the per mil difference from the $^{14}\text{C}/^{12}\text{C}$ ratio of the pre-industrial atmosphere by the conversion

$$\Delta^{14}\text{C} = (\text{model units} - 100) / 10 \quad (9)$$

By treating radiocarbon in this way, it is not necessary to know the precise value of the pre-industrial $^{14}\text{C}/^{12}\text{C}$ standard. However, for the purpose of computing inventories of bomb radiocarbon, the pre-industrial $^{14}\text{C}/^{12}\text{C}$ ratio is taken to be 1.176×10^{-12} (Siegenthaler, 1989). The gas exchange rate for radiocarbon follows the method used for CO_2 , and is either variable, according to the wind-speed dependent piston velocity computed in equation (7), or fixed at $0.067 \text{ moles } \mu\text{atm}^{-1} \text{ m}^{-2} \text{ yr}^{-1}$. The natural pre-industrial radiocarbon distribution was obtained by forcing the model with the fixed atmospheric $^{14}\text{C}/^{12}\text{C}$ ratio of 100 model units (equivalent to 0 ‰), and running the model to equilibrium. The carbon cycle model neglects the effect that biologically mediated fluxes of particulate carbon into the deep sea have on ^{14}C age, but the error associated with this is less than 10%, well within other uncertainties in determining absolute ages. Natural ^{14}C provides a useful indicator of the deep-sea ventilation characteristics of the ocean and its concentration gives an indication of the relative "ages" of different water masses. As well as natural radiocarbon, bomb radiocarbon was simulated by forcing the model with the observed atmospheric history from 1765 to 1990. Its transfer into the ocean following the large inputs into the atmosphere following nuclear weapons testing in the 1950's and 1960's has made it a useful tracer for studying atmosphere-ocean exchange and ocean circulation.

2.4 Experimental Procedure

Initial fields of temperature and salinity were set from the Levitus (1982) climatology, the concentration of dissolved inorganic carbon was initialised to a constant value of $2300 \mu\text{mol kg}^{-1}$, $\Delta^{14}\text{C}$ was set to -150 ‰ , and the model was spun up from a state of rest with seasonally varying climatological forcing (see section 2.1) using the spin-up acceleration technique described by Bryan (1984). The acceleration technique consists of distorting the model physics by taking a longer timestep for tracers than is used for the momentum equation and by taking longer timesteps at depth. This can be done because stability criteria are less severe for tracers and at depth within the ocean. The effect of the longer timestep at depth is to increase the effective integration time of the deep ocean relative to the surface. The technique introduces scaling factors into the time-dependent terms of the equations of motion, which tend towards zero as equilibrium is reached ($d/dt = 0$). Thus the equilibrium state of a model integrated using spin-up acceleration will be the same as that of a model integrated with standard time-stepping, provided that the forcing used is steady. For seasonally varying forcing these conditions are not satisfied exactly, but are approximated provided that the ratio between tracer and velocity time-steps is small enough to permit the model currents to adjust fully to variations in forcing, which occur on a monthly timescale in this case. A 1 day timestep for tracers with a 1 hour timestep for velocities is used, giving a distortion factor of 24. This technique results in a considerable saving in computer resources.

The model was spun up for 2000 surface years (equivalent to 8000 years in the deep ocean) with atmospheric $p\text{CO}_2$ held at a constant value of 278 ppm, corresponding to the value estimated for the period prior to the industrial revolution. By the end of the spin-up run the model property distributions had reached essentially steady state, the criterion adopted for determining whether the model was sufficiently spun up being that at all levels the rates of change of global temperature and salinity should be less than 0.02°C and 0.003 psu per century respectively, and that the net ocean-atmosphere carbon exchange should be less than 0.1 GtC yr^{-1} . The timestep acceleration factors were switched off for the last 200 years of the spinup, and remained off for subsequent runs.

Starting from this spinup the period from 1760 to 1990 was simulated using atmospheric concentration data from ice cores (Neftel *et al.*, 1985; Friedli *et al.*, 1986) and from atmospheric observations (Keeling *et al.*, 1989) prescribed as a boundary condition. Thus the model was run in "inverse mode" with atmospheric $p\text{CO}_2$ prescribed and fluxes being derived from the integration. The baseline integrations for the natural and anthropogenic carbon cycles employed the spatially-varying gas exchange formulation of Liss and Merlivat (1986). In addition, the simulation of the period 1765 to 1990 was repeated with the Liss and Merlivat gas exchange replaced with a constant gas transfer coefficient of $0.067 \text{ mole } \mu\text{atm}^{-1} \text{ m}^{-2} \text{ yr}^{-1}$. This run was initialised from the final state of a further 200 year spinup run with the new gas exchange. The purpose was to provide easier comparison with other models and to look at effect of a change in the gas transfer formulation on CO_2 and ^{14}C take-up.

A pair of runs were done from 1990 to 2300 using two different scenarios for future increases in atmospheric $p\text{CO}_2$ provided by the IPCC (Enting *et al.*, 1994). These scenarios stabilize at 450 ppm (S450), and 650 ppm (S650) respectively. The purpose of these runs was to deduce the level of emissions reduction required to stabilize atmospheric CO_2 concentrations at the given levels.

$\Delta^{14}\text{C}$ was included for the full duration of the run with the atmospheric value being held at 0‰ during the spin-up. After 1765 atmospheric $\Delta^{14}\text{C}$ was set to the historical values taken from direct measurements on CO_2 extracted from the air and from tree-ring data, using time-series provided by the IPCC (Enting *et al.*, 1994). The historical record after 1900 is shown in Figure 1. The model atmosphere was divided into three regions: ($> 20^\circ\text{N}$, 20°N to 20°S , $> 20^\circ\text{S}$), which biases the input slightly towards the Northern hemisphere. The forcing function includes the effect of a depletion in the amount of ^{14}C relative to ^{12}C that occurred prior to the 1950's due to dilution from the burning of large amounts of fossil fuel (the Suess effect). After 1955, the isotopic ratio increased dramatically as a result of the widespread fallout from atomic weapons tests, so much so that 1955 and 1965 the concentration of radiocarbon in the atmosphere was nearly doubled. After 1970, the distinction in atmospheric $\Delta^{14}\text{C}$ between different latitude bands is eradicated by mixing within the atmosphere.

3 RESULTS AND DISCUSSION

3.1 Pre-Industrial Steady-State Distributions

We first of all look at the simulation of the pre-industrial ocean carbon cycle, prior to the anthropogenic increases in CO₂, by examining the model fields at steady-state. Meridional sections of the zonally-averaged temperature and salinity in the Atlantic and Pacific oceans are shown in Figure 2, along with the global overturning streamfunction in Figure 3. Global average temperatures and salinities at each level from the model and as interpolated from observed values (Levitus, 1982) are shown in Table 1. Below 2000m, the temperature is more than 2 degrees too warm when compared with Levitus, although the vertical and meridional structure is well reproduced. The temperature error is about 1.5 °C in the deep Pacific and twice as large as this in the deep Atlantic. In the top 1000m the model thermocline is only slightly thicker than observed. Despite the warming, the simulation is far better than previous efforts using this model where a constant vertical diffusivity was used (Taylor, 1994; Murphy and Mitchell, 1995). Then it was found that the thermocline was either much too diffuse if a large diffusivity was employed, or else the deep water was too cold and lacked meridional structure if a small value was used. Perhaps not surprisingly, the use of a vertically-varying diffusivity leads to a more realistic simulation. The model's salinity field also looks more realistic than previously, particularly in the Pacific. The deep North Atlantic is slightly too salty but Antarctic Bottom Water (AABW) is close to the observed salinity of 34.7 psu. The improvement in AABW is due to the enhanced wintertime salinity forcing used at the surface. NADW is too warm and salty owing to the undue influence of the Mediterranean outflow parametrization. A salinity maximum centred at a depth of 1000m at 35 °N can be seen in Figure 2(b), which is not apparent in the Levitus data when averaged over the Atlantic basin. The simulated temperature in the Mediterranean Sea at the depth of the outflow is as much as 3.5 °C too warm and the simple mixing applied at the straits of Gibraltar exports too much of this water which also has the wrong T,S characteristics into the Atlantic. The sections through the Pacific do not show this feature and are much closer to observations. The meridional streamfunction (Figure 3) shows the typical "conveyor belt" pattern with water sinking to large depths north of 60N in the North Atlantic and close to the coast of Antarctica. Note that the NADW appears to sink deeper than in Taylor (1995), reaching depths of 3500m instead of 2000m as before and 12 Sv ($1 \text{ Sv} = 10^6 \text{ m}^2 \text{ s}^{-1}$) of NADW crosses the latitude of 30 S into the Southern Ocean, which is at the lower end of observational estimates ranging from 13.5 Sv (Gordon, 1986) to 20 Sv (Broecker, 1991). The strength of the meridional overturning cell due to convection close to Antarctica has increased slightly from 8 Sv to 10 Sv in the present model, but is far less than the values found in England's (1993) experiments. This is not too surprising, since England's experiments involved the relaxation of salinities at points adjacent to the coast of Antarctica to high-salinity wintertime values throughout the entire year, whereas in this study the enhanced salinities are applied only during the period of austral winter. The strength of AABW production in the present model is consistent with a rough estimate of 10Sv as an upper limit given by Olbers (1993). Despite the intermediate and deep North Atlantic being too warm and salty, the overturning circulation appears reasonable, and has if anything improved from what it was before.

Figure 4 shows the depth of the mixed layer during March and September, the months when the mixed layer is generally at its deepest. Surface water is mixed down to depths exceeding 1000m in the Norwegian and Labrador Seas during March in agreement with observations. In the southern hemisphere deep convection occurs intermittently during winter in the Ross and Weddell seas, causing properties to be well mixed adjacent to the Antarctic coast. There is a large region to the south-west of Australia where the winter-time mixing extends down to more than 500 metres, which is absent from observations. Elsewhere, the model's mixed layer depths agree quite well with the maps published by Levitus (1982, Figs 95a and 96a). There is a tendency for the model to over-predict mixed layer depths in the tropics, which may be related to the use of the Hellerman and Rosenstein wind stresses to force the model, since these are known to be too strong in this region. Generally, though, the model's seasonal mixing characteristics appear to be fairly representative of the real ocean.

Horizontal maps of the currents at depths of 5m, 100m and 2100m are shown in Figure 5. The surface current includes a strong Ekman component as well as the geostrophic velocity, and so the currents immediately below this top layer are more representative of the surface transports. The model generally reproduces most aspects of the large-scale circulation. The Gulf Stream and other jet-like currents tend to be much broader and weaker than observed due to the high viscosity required by the use of coarse resolution. This is not much of a problem for climate simulations, however, as the sluggishness of the currents is compensated for by the current occupying a wider area, so that the total transport of heat and other properties is approximately correct (Bryan, 1991). A southward-flowing deep western boundary current can be observed along the western side of the Atlantic at 2100m, representing the outflow of the model's NADW.

Figure 6 shows natural radiocarbon at the surface and along meridional sections through the Atlantic and Pacific oceans from the variable gas exchange run. Low surface values of $\Delta^{14}\text{C}$ are found close to the coast of Antarctica, where values as low as -130‰ are found in the Ross Sea. This is an improvement on the earlier version of this model, which gave younger values around Antarctica, but is still too high compared with observed values of -140 to -150‰ . $\Delta^{14}\text{C}$ is closest to the imposed atmospheric value in the subtropical gyres. There is good agreement with estimates of pre-1900 values of $\Delta^{14}\text{C}$ derived from measurements on corals collated by Toggweiler *et al* (1989a). The sections through the Atlantic and Pacific show that the oldest water with lowest values occur in the deep North Pacific where a core of water with $\Delta^{14}\text{C}$ of -250‰ lies between 1700 and 3500m depth. This is slightly older than was found in the GEOSECS data, where oldest waters were estimated at -240‰ . In the North Atlantic, NADW has $\Delta^{14}\text{C}$ ranging from -50 to -90‰ and fills the North Atlantic basin down to the bottom northwards of 30°N . Previous versions of this model had NADW confined to depths above 2000m. A tongue of lower $\Delta^{14}\text{C}$ water can be seen sandwiched between two slightly younger water masses at 1000m depth in the South Atlantic. This is the signature of Antarctic intermediate water. There is very good agreement with Geosecs observations below 1000m (ie deeper than the penetration of bomb radiocarbon which is present in the observations). Since Toggweiler *et al* (1989a) has shown that $\Delta^{14}\text{C}$ distribution simulated by a model is sensitive to the

vertical mixing used, this good agreement can be taken as evidence that on a global scale, vertical transport across the thermocline is being correctly represented in the model .

Figure 7 shows the model's pre-industrial atmosphere-ocean CO₂ flux from the run using the Liss and Merlivat (1986) gas exchange formulation. Air-sea exchange is influenced by sea surface temperature, upwelling of carbon-rich water from below the mixed layer, and wind- and convectively- induced surface mixing. Thus outgassing occurs in the warm waters of the tropics and is strongest in the tropical eastern Pacific, the Indian Ocean, and along the western coast of North America. The ocean absorbs CO₂ from the atmosphere in the colder waters to the north and south, with largest fluxes occurring in the northern North Atlantic, around the Southern oceans, and in the North-west Pacific.

3.2 Anthropogenic CO₂ Uptake, 1765-1990

Unless stated otherwise all of the following results are from spatially varying gas exchange run. Once steady-state was achieved, the model was used to simulate oceanic uptake of anthropogenically-produced CO₂ for the period 1765 to 1990. This was done by forcing the model's atmospheric CO₂ reservoir to follow the observed history of CO₂ concentration shown in Figure 8. Atmospheric CO₂ concentration starts at 278 ppm in 1765, increasing approximately exponentially to 353 ppm in 1990. Time-series of the total oceanic CO₂ fluxes derived from this procedure are shown in Figure 9, which also breaks the fluxes down into regions. The net flux at the start of the run ($-0.05 \text{ GtC yr}^{-1}$) is not quite zero, indicating that the model, is close to, but not quite, in equilibrium. In the pre-industrial era, the low latitudes act as sources of CO₂ which are balanced by sinks at high latitudes. As the atmospheric perturbation increases, the low latitude sources reduce in strength until by 1990 the net flux from these regions is close to zero. Global CO₂ flux increases gradually until 1950, after which time the uptake by the ocean accelerates. At the end of the experiment in 1990, the ocean is taking up 2.24 GtC yr^{-1} . The average uptake for the decade 1980-1989 is 2.0 GtC yr^{-1} , and the total uptake from 1794 to 1990 is 98.6 GtC . The CO₂ uptake rate is slightly higher than that obtained with the Princeton model (Sarmiento *et al*, 1992), and considerably higher than in the Hamburg model (Enting *et al*, 1994). As such, the uptake rate lies in the middle of the range of current IPCC estimates of $2.0 \pm 0.8 \text{ GtC yr}^{-1}$ for the 1980's (IPCC, 1994). Figure 10 shows timeseries of the perturbation CO₂ flux (defined as the difference from the flux in 1765) for different regions. The perturbation fluxes are shown as the percentage of the total excess flux. A large proportion (65%) of the uptake takes place in the southern hemisphere with a further 25% being contributed by the Northern hemisphere tropics and subtropics. Of the relative southern hemisphere uptake of 65%, 34% occurs south of 45°S and 31% is taken up in the region extending from 45°S to the equator. The high latitude Atlantic and Pacific oceans are rather small sinks for anthropogenic CO₂. This is hardly surprising for the North Pacific, but the North Atlantic is a region where a large proportion of the world's deep water is produced and where properties introduced at the surface can be rapidly transported to depth. The small contribution of the North Atlantic to global CO₂ uptake is a consequence of its small surface area, as is illustrated by Figure 11. This shows the spatial distribution of the annually-averaged perturbation flux, and it can be seen that the North Atlantic subpolar gyre and the convective zone

to the northwest of Scandinavia are regions of quite intense CO₂ uptake. Another region of intense fluxes lies in a band between 50 °S and 70 °S extending right around the globe along the Antarctic polar front.

It was mentioned earlier in this paper that two parallel runs were performed. The main set of experiments used a spatially varying gas exchange based on the Liss and Merlivat formulation, while an additional experiment used a fixed transfer coefficient but was in all other respects identical to the first. Figure 12 compares the global CO₂ fluxes from the two runs, from which it can be seen that the effect of varying the transfer coefficient on CO₂ uptake is minimal, the uptake rates in 1990 being almost indistinguishable. This is in accord with Sarmiento *et al*'s (1992) findings using a 3D model and with earlier experience with simple 1D models. In all these earlier experiments, the models used did not include seasonal variations. The present model includes a seasonally varying mixed layer depth, and seasonal changes in gas exchange coefficient and CO₂ solubility, yet the same insensitivity of CO₂ to gas exchange formulation is found. Locally, there are some differences between the instantaneous fluxes (Figure 13) from the two runs with differences as high as 0.6 mole m⁻² yr⁻¹, but areas of increased CO₂ uptake are compensated for by areas of increased CO₂ loss so that the global effect is negligible. However, the geographical variability means that choice of gas exchange formulation will have a large effect on comparisons between model and observed fluxes. For this reason, we have chosen not to compare the model simulation with the estimates of air-sea CO₂ fluxes based on observations (Tans *et al*, 1990).

Another reason for not doing the comparison is the neglect in the model of the effect of ocean biota on CO₂ fluxes. Not only will pCO₂ be overestimated in the duration of a phytoplankton bloom, but pCO₂ will also be underestimated in upwelling areas due to the underestimate of the vertical gradients of TCO₂. The former effect is illustrated by Figure 14 which shows the annual cycle of primary production and pCO₂ at a site in the North Atlantic, taken from a more recent version of the model which includes the biological pump. During the spring phytoplankton bloom when production reaches a peak of 1.3 gC m⁻² d⁻¹ in this model, pCO₂ falls temporarily by almost 50 µatm and remains below the atmospheric value throughout the summer. Also shown in Figure 14 is the modelled pCO₂ at the same site when the biological pump is ignored. In this case, in the absence of the bloom, pCO₂ rises over the course of the summer in line with sea surface temperature, resulting in outgassing of CO₂ to the atmosphere during summer and autumn. While the absence of the biological pump from the model clearly makes a comparison of modelled pCO₂ against observed pCO₂ meaningless, it should be noted that its neglect will have little influence on this paper's conclusions. The results discussed in this paper concern the uptake of excess CO₂ from the atmosphere, where "excess" refers to the anthropogenic perturbation to the natural (or pre-industrial) carbon cycle, under the assumption that the ocean circulation remains unchanged and that no other feedbacks occur to any significant extent. In these circumstances it can be assumed that the ocean biota will operate in exactly the same way in both the natural and the perturbed systems and the biological pump will thus have little effect on estimates of the uptake of excess CO₂.

A method of comparison with observation which is not compromised by the neglect of the biological pump and a sensitivity to gas exchange formulation is offered by calculations of the inventory of excess CO₂ provided by Chen (1993). The method used by Chen consists of estimating the TCO₂ content before the onset of the industrial revolution by correcting deep water TCO₂ content for changes that have occurred since the sample was last at the surface, due to the oxidation of organic matter and changes in alkalinity. The accuracy offered by this technique has been much criticised, due to uncertainty in estimating winter values at the surface (Broecker *et al*, 1985b) and problems caused by mixing of water masses (Shiller, 1981, 1982). Nevertheless it provides a direct estimate of CO₂ uptake with which to independently compare models, and the collection of winter-time data would help improve these estimates (Wallace, 1995). The inventories obtained by this technique are compared with the model estimates for the year 1980 in Table 2. Overall the modeled uptake (93.1 GtC) is only slightly larger than the observed figure of 82.3, and lies within the estimated uncertainty. In the Northern Hemisphere the model inventories are within the error bars of the data, but in the Southern Hemisphere the model appears to have taken up somewhat more CO₂ than is suggested by the observations. The uncertainties just discussed prevent us from drawing any further conclusions, but the data hint that the Southern Ocean CO₂ uptake predicted by the model should be examined more closely. We will return to this question in the section on bomb radiocarbon validation.

3.3 Future CO₂ Emission Targets

An assessment of the future levels of CO₂ emissions needed to achieve given target atmospheric CO₂ concentrations is of importance to policymakers tasked with negotiating agreements on future greenhouse gas emissions. We have used the ocean carbon cycle model to provide estimates of these emissions for two different scenarios: atmospheric CO₂ stabilising at 450ppm by the year 2100 (scenario S450), and at 650ppm by year 2200 (scenario S650). The first scenario corresponds to ultimate CO₂ levels being approximately 25% higher than the present day, or about 60% higher than pre-industrial. The second target is about 2.3 times the pre-industrial value. These two concentration profiles were taken from Enting *et al* (1994) and were chosen to give a smooth transition between the 1990 rate of CO₂ increase and the value at stabilisation. Required emissions were obtained by running the model from year 1990 to 2300 with atmospheric pCO₂ being forced to follow the curves shown in Figure 15. The resultant net atmosphere-ocean CO₂ fluxes were used to compute the net emissions into the atmosphere as the sum of the flux into the ocean and the accumulation in the atmosphere implied by the concentration profiles in Figure 15. These net emissions represent the combined effect of fossil fuel input, release of CO₂ due to land-use changes or deforestation, and a sink due to enhanced growth of the terrestrial biosphere in conditions of increasing CO₂. Climatological forcing was used throughout the experiment, and so any possible changes in CO₂ uptake due to shifting climate patterns have not been considered in these runs.

Figure 16 shows the global oceanic CO₂ uptake and the corresponding net CO₂ emissions for the two scenarios. The sharp kinks in the net emission curves at years 2100 (for S450) and 2200 (for S650) are due to the atmospheric accumulation rates (as implied by the stabilisation histories) falling to zero at these times. Thereafter, net emissions is equal to ocean

uptake by definition. For the low pCO₂ scenario S450, oceanic flux reaches a maximum of 2.66 GtC yr⁻¹ in 2020, before declining to about 1.7 GtC yr⁻¹ by the end of the next century. This implies that the net emissions must start to decrease immediately from present levels of about 6 GtC yr⁻¹ to between 1 and 2 GtC yr⁻¹ over the course of the next century to achieve the target. The higher pCO₂ scenario S650 has oceanic uptake increasing to 3.6 GtC yr⁻¹ by 2060, and being maintained at this level for the remainder of the next century. Thereafter, oceanic uptake declines to about 1.7 GtC yr⁻¹ by the year 2300. The resulting effect on net emissions is that they could be allowed to reach as high as 7.8 GtC yr⁻¹ by the middle of the next century, but would have to decline sharply thereafter if the target is to be met. By year 2200 at the latest total net emissions would have to be close to the 2.0 GtC yr⁻¹ mark.

We have also converted the estimated net emissions into estimates of the fossil fuel emissions alone. This was done by removing the deforestation and terrestrial sink components from the net emissions plotted in Figure 16b. The terrestrial sink was computed as the residual required to balance the carbon budget, given that the other components of the carbon cycle are either known or can be estimated for the period 1765 to 1990. In other words, the carbon cycle is assumed to satisfy the following equation:

$$2.123 \, d(C)/dt = Q_{\text{foss}}(t) + D_n(t) - S_{\text{ocean}}(t) - S_{\text{fert}}(t) \quad (10)$$

where $C(t)$ is the atmospheric concentration, Q_{foss} is the industrial emissions source (including contributions from cement production), D_n is the source due to anthropogenic land use changes and deforestation, and S_{ocean} and S_{fert} are the oceanic and terrestrial sinks respectively. The factor 2.123 GtC/ppm converts between atmospheric concentration and inventory. $C(t)$ was prescribed as a spline fit to the observations referenced in section 2.4. The data for Q_{foss} were those given by Keeling (1991) and Marland and Boden (1991) with a linear extrapolation back to zero in 1844 from the start of the published record. D_n was taken as the data supplied to the IPCC by R.A. Houghton (Enting *et al*, 1994). S_{ocean} was computed by the model, leaving S_{fert} as the missing sink required to close the budget over this period. Figure 17 shows this estimated terrestrial sink as a function of time. Also shown are the land-use change data. We fitted a variety of functional forms to these data to describe the relationship between the response of the terrestrial biota and elevated CO₂ levels. Three different relationships were used: linear, logarithmic, and logistic:

$$S_{\text{fert}}(t)/S_{\text{fert}}(0) = \Theta_1 (C(t)/C(0)) + \Theta_2 \quad (11a)$$

$$S_{\text{fert}}(t)/S_{\text{fert}}(0) = \Theta_1 \log(C(t)/C(0)) \quad (11b)$$

$$S_{\text{fert}}(t)/S_{\text{fert}}(0) = \Theta_1 \tanh(\Theta_2(C(t)/C(0) + \Theta_3)) \quad (11c)$$

where (0) refers to the initial values in 1760. Θ_1 , Θ_2 and Θ_3 are the fitted parameters.

The functions were fitted by non-linear regression on the data up until 1990, yielding a least-squares estimate of the parameters θ_1 , θ_2 and θ_3 . The following values were obtained:

Linear	$\theta_1=45.3, \theta_2=-46.3$
Logarithmic	$\theta_1=40.6$
Logistic	$\theta_1=9.56, \theta_2=14.92, \theta_3=-1.08$

The results of balancing the carbon budget by fitting the three different functional forms to the missing sink data are shown in Figure 18. None of the relationships provides an entirely satisfactory fit to the entire data record. The logistic function appears to match the most recent data better than the other two functions used.

These functions were then used to predict the strength of the biospheric sink post-1990 for the two increasing CO₂ scenarios. The deforestation source post-1990 was taken as the IPCC 1992a* deforestation scenario (Enting *et al*, 1994). The fossil fuel source required to achieve the target atmospheric CO₂ concentrations was then calculated from equation 11. Figure 19 compares the projected fossil fuel emission targets under the above assumptions. The linear biosphere fertilization model assumes an ever increasing uptake by the land biota, and is likely to be excessively optimistic. Nevertheless it provides an upper bound on the target emissions. Even under this scenario, fossil fuel emissions could not rise more than 25-30% above present-day values if stabilisation at 450ppm were to be achieved. The logistic model assumes that the CO₂ fertilisation mechanism will saturate at a certain CO₂ concentration, beyond which the mechanism becomes ineffective. The fit to the data pre-1990 implies that this level has been reached and so effectively the model assumes that the terrestrial sink is unchanging beyond 1990. This is the most pessimistic scenario of the three. Under this assumption, fossil fuel emissions would have to begin falling by the year 2000 and would have to be cut to half their present levels by the end of the next century if atmospheric pCO₂ were to stay below 450ppm. Even the 650ppm target would be difficult to achieve since it would require fossil fuel input to peak at no more than 9 GtC yr⁻¹, or 50% higher than today. If the terrestrial sink were to increase in the future, then there would be considerably more leeway for achieving the target values of pCO₂, particularly for the higher ones. The large spread in permitted fossil fuel emissions at stabilisation is illustrative of the high degree of uncertainty attached to our present knowledge of the land carbon cycle, and the effect this has on our estimates. It will be very important to reduce this uncertainty.

3.4 Simulation Of Bomb Radiocarbon

Validation of carbon cycle models is of paramount importance if the models are to be used to obtain credible estimates of future CO₂ uptake, but direct validation against observations is difficult due to uncertain knowledge of the actual fluxes of CO₂, and large temporal and spatial variability in pCO₂. A comparison between the modelled and observed inventories of TCO₂ was presented in section 3.2, where it was noted that the observed estimates were still quite uncertain. The

comparison hinted that the uptake of CO₂ in the model may be too strong. An alternative method of testing the veracity of a carbon cycle model is by using it to simulate the uptake of bomb radiocarbon. The slow transfer of bomb radiocarbon into the ocean following the large input into the atmosphere due to nuclear weapons tests during the 1950's and 1960's has made it a useful tracer for atmosphere-ocean exchange and ocean circulation. It provides a test of the models uptake characteristics on a timescale of years to decades, which is an appropriate timescale for the CO₂ problem, and is not affected by small-scale and short term variations in surface values. Furthermore, an extensive set of observations of $\Delta^{14}\text{C}$ exists, and this data set is being added to as part of the WOCE program. Water column inventories of bomb radiocarbon good to between 5% and 10% have been constructed (Broecker *et al*, 1985a) which can be compared against model-derived inventories and our knowledge of the atmospheric $\Delta^{14}\text{C}$ history is good, so the boundary condition for ^{14}C is well-known. It should be borne in mind, though, that $\Delta^{14}\text{C}$ is not a direct analogue of CO₂. Its rate of transfer across the air-sea interface is an order of magnitude slower than CO₂ and so this method of validation does not test the model on seasonal timescales. Also, the input of radiocarbon into the atmosphere occurred rather rapidly compared with the gradual build up of CO₂

The Suess effect (Suess, 1955) present in the atmospheric forcing function is mirrored by the surface ocean in the model. Deficits of ^{14}C in 1950 relative to 1850 of -10 ‰ in the Gulf of Mexico and Caribbean Sea and -6 ‰ in the tropical eastern Pacific are consistent with measurements made on Pacific and Atlantic corals of -11‰ (Florida), -12‰ (Belize) and -6‰ (Galapagos) (Druffel, 1981; Druffel and Suess, 1983).

A map of the model depth-integrated water column inventory at the time of the Geochemical Ocean Sections Study (GEOSECS) for the run with spatially varying gas exchange is shown in Figure 20. Highest inventories occur in the subtropical gyres and the Labrador and Greenland-Iceland-Norwegian seas. The pattern agrees reasonably well with GEOSECS data, but can be as much as 25‰ lower than observations in the locations of the highest values. In contrast, the run with constant gas exchange (not shown) tends to be between 10 and 20% higher than the GEOSECS observations. Table 3 summarises this information and provides a comparison of inventories for various regions with GEOSECS observations and with the models of Stocker *et al* (1994) and Toggweiler *et al* (1989b). Overall there is fair agreement of run CBYQ (constant gas exchange) with observations, although inventories appear to be too high in the tropical Atlantic and Southern Ocean, and too low in the northern Atlantic. Inventories calculated with this model are in general higher than the models of both Stocker *et al* (1994) and Toggweiler *et al* (1989b). Comparison of the two runs made using the Hadley Centre model demonstrates the large effect that the gas exchange formulation has on inventory estimates. This is unlike the situation for CO₂, where we found that uptake was insensitive to the details of gas exchange. The Liss and Merlivat formulation with Hellerman winds gives much lower inventories than the fixed gas exchange run. In fact, the two runs predict values of the mean concentration of bomb ^{14}C in surface water of 142 ‰ and 200 ‰ respectively, which bracket the observed value of 160 ± 15 ‰ (Broecker *et al*, 1985a), both estimates lying beyond the limit of observational

uncertainties. This illustrates the difficulty of making meaningful comparisons between different models which may have very different gas exchange parametrizations. To avoid this problem we calculated bomb ^{14}C penetration depths by dividing the inventories by surface concentrations. The penetration depth thus obtained is a measure of vertical transport and excludes the influence of gas exchange. Table 4 compares penetration depths for the various models and for observations. There is generally good agreement with observation, even in regions such as the tropical Atlantic where the inventory was too high. It is particularly noticeable from these tables, however, that the vertical penetration of radiocarbon into the Southern Ocean in the model is much higher than observations would indicate, regardless of the type of gas exchange used. The model predicts a depth scale of 570m, compared with 330m observed during GEOSECS. The implication is that the model's vertical exchange in the Southern Ocean is over-vigorous, and the uptake of gases in this region is excessive, as was hinted at by the comparison with excess CO_2 inventories discussed earlier. As 35% of the global uptake of excess CO_2 takes place in water south of latitude 45S, the over-strong uptake in this region introduces quite a large element of uncertainty into our predictions, which it will be important to address in future versions of the model. Elsewhere, the vertical transport in the model appears to be functioning correctly.

3.5 Sensitivity of Results To The Parametrisation Of Mediterranean Outflow

In section 3.1 it was noted that the method used to parametrise the outflow of water from the Mediterranean basin resulted in intermediate and deep water masses in the North Atlantic that were warmer and saltier than observed. To test the effect of the overstrong parametrization of the Mediterranean outflow on our results, we repeated the spinup and historical CO_2 uptake experiment with the Mediterranean outflow switched off. Figure 21 shows profiles of the globally averaged temperatures and salinities at each level from this run. Also shown are the corresponding profiles from the Levitus dataset and from the standard run including the Mediterranean outflow. There is now an exceptionally good agreement with observations for temperature with the bias in deep water being almost completely removed. Unfortunately, the simulation of global average deep and intermediate salinities is made worse by the removal of the outflow. The effect that this has on the overturning circulation (not shown) is to weaken slightly the cell associated with NADW and cause it to lie at a somewhat shallower depth. The flow of water from this cell crossing the equator is reduced from 8Sv to 4Sv. In the Southern Hemisphere the deep water cell centred just south of the equator is also weaker, but the circulations that are connected to the surface are unaffected by the change. The important outcome for this study is that the weakening of the deep water circulation occasioned by the removal of the outflow parametrisation has very little effect on CO_2 uptake. The average uptake for the period 1980-89 is increased slightly to 2.05 GtC yr^{-1} in the run without Mediterranean outflow, compared with 2.0 GtC yr^{-1} in the run with the outflow, and the distribution of the excess flux between different ocean areas is unchanged.

3.6 The Effect of the Strong Deacon Cell on Tracer Uptake

It was shown in section 3.4 that in the Southern Ocean south of 40S, the bomb radiocarbon- derived penetration depths for the model are almost double what the observations of ^{14}C suggest. We will therefore use observations of the freon F11 to investigate this issue further. Freons are in many ways an ideal tracer for observing ocean ventilation. They are inert, unaffected by biological processes, and have been injected into the ocean over a period comparable with that of the rapid increase in CO_2 over the past 50 years (Figure 22). Difficulties in measuring their concentration in seawater has meant that up till now they have received relatively little attention as verification tools for ocean models. Recently it has become much easier to make these measurements (Bullister and Weiss, 1988), and as more observations become available modellers have started to investigate their use (eg. England, 1995; Robitaille and Weaver, 1995; Roether *et al*, 1993).

The model simulations for the period 1950 to 1990 included the freons F11 and F12 as additional tracers. The atmospheric concentrations (Figure 22) were imposed as a boundary condition and transfer into the ocean calculated according to the difference between the actual surface concentration and the concentration at saturation using a gas exchange formulation similar to that used for CO_2 . The solubilities for F11 and F12 used for determining saturations were computed using the formulae given by Warner and Weiss (1985).

Figure 23a shows the distribution of F11 along the Greenwich meridian as observed during late 1983. The corresponding data from the model are shown in Figure 24b. Near to the surface, and north of 50 °S there is good agreement between model and observations. South of this latitude there appears to be much too much penetration of F11 from the surface. This is made very clear by following the 0.8 pmol kg^{-1} isoline. Instead of reaching a maximum depth of 1000m at 45 °S and rising back towards the surface south of this latitude, the model shows the isoline as continuing to deepen to reach 1600m at 63 °S, so that the penetration of this particular isoline appears to be much deeper than is observed at this particular latitude. The implication is that between the latitudes of 45 °S and 65 °S the model's vertical transfer of CO_2 , heat and other tracers is much too strong, resulting in an overestimation of the strength of the oceanic sink in this region. The latitude range over which this occurs coincides with the position of the strong Deacon cell of strength 26 Sv (centred at 45 °S) in the meridional streamfunction (Figure 3). Robitaille and Weaver (1995) and England (1995) have compared the Gent and McWilliams (1990) scheme for isopycnal diffusion with the standard isopycnal scheme used for these experiments. They found that the Gent and McWilliams scheme resulted in a marked reduction in the strength and maximum depth of the Deacon cell and a substantial improvement in the deep ocean F11 distribution. The implication for this work is that the present model, in common with most other coarse resolution GCMs which use either horizontal diffusion or isopycnal diffusion, overestimates the uptake of heat, CO_2 and other tracers in the Southern Ocean. We plan to introduce the Gent and McWilliams parametrisation into our model in the near future, and will obtain revised estimates of anthropogenic CO_2 uptake. We expect that the uptake in the Southern Ocean will be reduced by the introduction of the new scheme.

4 CONCLUSIONS

We have described the Hadley Centre ocean carbon cycle model. This model is based on the Hadley Centre ocean circulation model, with the addition of tracer and carbon cycle components. The version of the model used in the present experiments considers only the inorganic component of the ocean carbon cycle. The model was used to simulate the pre-industrial steady-state carbon cycle and its response to increases in atmospheric CO₂ under the assumption of an unchanging ocean circulation. The circulation characteristics of the model appear reasonable, but the deep water is too warm. This is associated with the undue influence of the parametrisation of Mediterranean outflow used. It was shown that the removal of the Mediterranean outflow eliminated the models warm bias, but had negligible effect on CO₂ uptake.

The model takes up an average of 2.0 GtC yr⁻¹ for the decade 1980-1989, a figure which lies at the centre of the range of current IPCC estimates. The majority of the uptake occurs in the Southern hemisphere, with 35% of the global uptake taking place south of 45 °S. In contrast, the high Northern latitudes are small, but intense, sinks. Comparison of the models inventory of anthropogenic CO₂ with observationally-based estimates suggests that the Southern Ocean CO₂ uptake is over-estimated, perhaps by as much as 50% in the South Pacific ocean. Both natural and bomb radiocarbon data were used to help validate the model. The natural radiocarbon distribution shows good agreement with GEOSECS data below 1000m, as does the uptake of bomb-radiocarbon in most regions of the globe. However, excessive uptake of tracers in the Southern Ocean is confirmed by both the calculation of bomb radiocarbon penetration depth, which is 75% higher than the observational estimate at the time of GEOSECS, and by the simulation of the distribution of the chlorofluorocarbon F-11. This points to a weakness in the present model, which appears to be common to many other circulation models used for climate studies. We anticipate that the introduction of a new scheme for along-isopycnal mixing will go some way to alleviating the problem, although it may also be necessary to improve the parametrisation of convection used in the model. We also found that anthropogenic CO₂ uptake was insensitive to details of the gas exchange parametrisation, thus extending the findings of Sarmiento *et al* (1992) to the case of seasonally varying forcing, CO₂ solubility, gas exchange coefficient and mixed layer depth.

We used the model to obtain estimates of the future levels of CO₂ emissions required to achieve target atmospheric CO₂ concentrations of 450 ppm and 650ppm. We found that net emissions of CO₂, comprising the individual contributions from fossil fuel, land-use changes and enhanced growth of the land biosphere, would have to decline immediately from present levels of nearly 6 GtC yr⁻¹ to less than 2 GtC yr⁻¹ by the end of the next century in order to achieve the 450ppm stabilisation target. In the case of the 650ppm scenario, net emissions could be permitted to rise to nearly 8 GtC yr⁻¹ by the middle of the next century, but would have to decline to less than 2.5 GtC yr⁻¹ by the end of the following century. In both

cases, the ultimate level of emissions is required to be substantially lower than at present.

The experiments described in this paper have all assumed that the circulation of the ocean is unchanging, and have neglected the response of the ocean to increases in greenhouse gas forcing, and the corresponding effects that this may have on CO₂ uptake. Proper investigation of these effects requires the use of a coupled ocean-atmosphere model, which in turn requires the development of a model of ocean biology and the organic carbon pump. We are currently working on the inclusion of a simple ecological model, which will enable us to compare model results directly against observations of surface pCO₂, and to investigate the role of various feedback mechanisms involving circulation changes and changes in biogeochemical cycling.

ACKNOWLEDGEMENTS

Thanks are due to Dr Y. L. Jia for information on CFCs.

The work described in this article was carried out at the Hadley Centre for Climate Prediction and Research under the UK Department of the Environment Climate Prediction Programme (contract PECD 7/12/37).

REFERENCES

- Bacastow, R.B. (1981). Numerical evaluation of the evasion factor. In Carbon Cycle Modelling, edited by B. Bolin, pp 95-101, John Wiley, New York.
- Bottomley, M., Folland, C.K., Hsiung, J., Newell, R.E., and Parker, D.E. (1990). Global ocean surface temperature atlas (GOSTA). A joint project of the Meteorological Office and Dept. of Earth, Atmospheric and Planetary Sciences, Massachusetts Institute of Technology. HMSO, London, 333pp.
- Broecker, W.S. (1991). The Great Ocean Conveyor. *Oceanography*, 4, 79-89.
- Broecker, W.S., Peng, T.-H., Ostlund, G., and Stuiver, M. (1985a). The distribution of bomb radiocarbon in the ocean. *J. Geophys. Res.*, 90, 6953-6979.
- Broecker, W.S., Takahashi, T., and T.-H. Peng. (1985b). Reconstruction of past atmospheric CO₂ contents from the chemistry of the contemporary ocean. US Dept. Energy Report DOE/OR-857. 79pp.
- Bryan, K. (1969). A numerical method for the study of the circulation of the world ocean. *J. Comput. Phys.*, 4, 347-379.
- Bryan, K. (1984). Accelerating the convergence to equilibrium of ocean climate models. *J. Phys. Oceanogr.*, 14, 666-673.
- Bryan, K. (1991). Poleward heat transport in the ocean. A review of a hierarchy of models of increasing resolution. *Tellus*, 43AB, 104-115.
- Bryan, K., and Cox, M.D. (1972). An approximate equation of state for numerical models of ocean circulation. *J. Phys. Oceanogr.*, 2, 510-514.
- Bullister, J.L., and Weiss, R.F. (1988). Determination of CCL₃F and CCL₂F₂ in seawater and air. *Deep-Sea Research*, 35, 839-853.
- Chen, C.-T. (1993). The oceanic anthropogenic CO₂ sink. *Chemosphere*, 27, 1041-1064.

- Cox, M.D. (1984). A primitive equation, 3-dimensional model of the ocean. GFDL Ocean Group Tech. Rep. No. 1, 143pp.
- Cox, M.D. (1987). Isopycnal Diffusion in a z-coordinate ocean model. *Ocean Modelling*, 74, 1-5.
- Druffel, E.M. (1981). Radiocarbon in annual coral rings from from the eastern tropical Pacific Ocean. *Geophys. Res. Lett.*, 8, 59-62.
- Druffel, E.M., and Suess, H.E. (1983). On the radiocarbon record in banded corals: Exchange parameters and net transport of $^{14}\text{CO}_2$ between atmosphere and surface ocean. *J. Geophys. Res.*, 88, 1271-1280.
- England, M.H. (1993). Representing the global-scale water masses in ocean general circulation models. *J. Phys. Oceanogr.*, 23, 1523-1552.
- England, M.H. (1995). Using chlorofluorocarbons to assess ocean climate models. Submitted to *Geophysical Research Letters*.
- Enting, I.G., Wigley, T.M.L., and Heimann, M. (1994). Future emissions and concentrations of carbon dioxide: key ocean/atmosphere/land analyses. CSIRO. Division of Atmospheric Research Technical Paper No. 31.
- Esbensen, S.K., and Kushnir, Y. (1981). The heat budget of the global ocean: An atlas based on estimates from surface marine observations. Climate Research Institute, Rep. No. 29, Oregon State University, Corvallis, USA.
- Etcheto, J., and Merlivat, L. (1988). Satellite determination of the carbon dioxide exchange coefficient at the ocean-atmosphere interface: A first step. *J. Geophys. Res.*, 93, 15669-15678.
- Friedli, H., Lotscher, H., Oeschger, H., Siegenthaler, U., and Stauffer, B. (1986). Ice core record of $^{13}\text{C}/^{12}\text{C}$ ratio of atmospheric CO_2 in the past two centuries. *Nature*, 324, 237-238.
- Gent, P.R., and McWilliams, J.C. (1990). Isopycnal mixing in ocean circulation models. *J. Phys. Oceanogr.*, 20, 150-155.
- Gerdes, R., Koberle, C., and Willebrand, J. (1991). The influence of numerical advection schemes on the results of

- ocean general circulation models. *J. Climate*, 5, 211-226.
- Gordon, A.L. (1986). Interocean exchange of thermocline water. *J. Geophys. Res.*, 91, 5037-5046.
- Goyet, C., and Poisson, A. (1989). New determination of carbonic acid dissociation constants in seawater as a function of temperature and salinity. *Deep Sea Res.*, 36, 1635-1654.
- Haney, R.L. (1971). Surface thermal boundary condition for ocean circulation models. *J. Phys. Oceanogr.*, 1, 241-248.
- Hellerman, S., and Rosenstein, M. (1983). Normal monthly wind stress over the world ocean with error estimates. *J. Phys. Oceanogr.*, 13, 1093-1104.
- Jaeger, L. (1976). Monatskarten des Niederschlags fur die Ganze Erde. *Ber Deutsch Wetterdienstes*, 18, no. 139.
- Kraus, E.B., and Turner, J.S. (1967). A one-dimensional model of the seasonal thermocline. II. The general theory and its consequences. *Tellus*, 19, 98-105.
- Keeling, C.D. (1991). CO₂ emissions -historical record. In: Boden, T.A., Sepanski, R.J., and Stoss, F.W. (eds.) A compendium of global change. Carbon Dioxide Information Analysis Center, Oak Ridge National Laboratory, Oak Ridge, Tenn.
- Keeling, C.D., Bacastow, R.B., Carter, A.F., Piper, S.C., Whorf, T.P., Heimann, M., Mook, W.G., and Roeloffzen, H. (1989). A three dimensional model of atmospheric CO₂ transport based on observed winds. 1. Analysis of observational data. In: D.H. Peterson (ed.). *Aspects of Climate Variability in the Pacific and the Western Americas*. pp165-236, AGU, Washington, D.C.
- Kraus, E.B. (1988). Diapycnal mixing. In *Climate-Ocean Interaction*, edited by M.E. Schlesinger, pp 269-293, Oxford.
- Levitus, S. (1982). *Climatological Atlas of the World Ocean*, NOAA Professional Paper 13, U.S. Dept. of Commerce, 173pp.
- Liss, P., and Merlivat, L. (1986). Air-sea gas exchange rates, introduction and synthesis. In *The Role of Air-Sea Exchange*

in Geochemical Cycling, edited by P. Buat-Menard, pp 113-128, D.Reidel, Dordrecht .

Maier-Reimer, E., and Hasselmann, K. (1987). Transport and storage of CO₂ in the ocean - an inorganic ocean-circulation carbon cycle model. *Clim. Dyn.*, 2, 63-90.

Manabe, S., and Stouffer, R. (1988). Two stable equilibria of a coupled ocean-atmosphere model. *J. Climate*, 1, 841-866

Marland, G., and Boden, T. (1991). CO₂ emissions - modern record. pp386-389 of *Trends '91: A Compendium of Global Change*. Edited by T.A. Boden, R.J. Sepanski, and F.W. Stoss. Carbon Dioxide Information Analysis Center, Oak Ridge National Laboratory, Oak Ridge, Tenn.

Mehrbach, C., Culberson, C.H., Hawley, J.E., and Pytkowicz, R.M. (1973). Measurement of apparent dissociation constants of carbonic acid in seawater at atmospheric pressure. *Limnol. Oceanogr.*, 18, 897-907.

Murphy, J. M., and Mitchell, J.F.B. (1995). Transient response of the Hadley Centre coupled ocean-atmosphere model to increasing carbon dioxide. Part I. Control climate and flux correction. *J. Climate*, 8, 36-80

Neftel, A., Moor, E., Oeschger, H., and Stauffer, B. (1985). Evidence from polar ice cores for the increase in atmospheric CO₂ in the past two centuries. *Nature*, 315, 45-47.

Olbers, D. (1993). Links of the Southern Ocean to the Global Climate. In: *Modelling Ocean-Climate Interactions*, edited by J. Willebrand and D.L.T. Anderson. pp 205-241. Springer-verlag, Berlin.

Oeschger, H., Siegenthaler, U., Schotterer, U., and Gugelmann, A. (1975). A box diffusion model to study the carbon dioxide exchange in nature. *Tellus*, 27, 168-192.

Pacanowski, R.C., and Philander, S.G.H. (1981). Parametrization of vertical mixing in numerical models of tropical oceans. *J. Phys. Oceanogr.*, 11, 1443-1451.

Paulson, C.A., and Simpson, J.J. (1977). Irradiance measurements in the upper ocean. *J. Phys. Oceanogr.*, 7, 952-956.

Peng, T-H., Takahashi, T., and Broecker, W. (1987). Seasonal variability of carbon dioxide, nutrients and oxygen in the

- northern North Atlantic surface water: observations and a model. *Tellus*, **39B**, 439-458.
- Rahmsdorf, S. (1993). A fast and complete convection scheme for ocean models. *Ocean Modelling*, **101**, 9-11.
- Redi, M.H. (1982). Oceanic isopycnal mixing by coordinate rotation. *J. Phys. Oceanogr.*, **12**, 1154-1158.
- Robitaille, D.Y. and Weaver, A.J. (1995). Validation of sub-grid scale mixing schemes using CFCs in a global ocean model. Submitted to *Geophysical Research Letters*.
- Roether, W., Roussenov, V.M., and Well, R. (1993). A tracer study of the thermohaline circulation of the Eastern Mediterranean. In: *Ocean Processes in Climate Dynamics: Global and Mediterranean Examples*. Kluwer.
- Sarmiento, J.L., Orr, J.C. and Siegenthaler, U. (1992). A perturbation simulation of CO₂ uptake in an ocean general circulation model. *J. Geophys. Res.*, **97**, 3621-3645.
- Shiller, A.M. (1981). Calculating the oceanic CO₂ increase: a need for caution. *J. Geophys. Res.*, **86**, 11083-11088.
- Shiller, A.M. (1982). Reply to "Comment on calculating the oceanic CO₂ increase: a need for caution" by A.M. Shiller. *J. Geophys. Res.*, **87**, 2083-2085.
- Siegenthaler, U. (1983). Uptake of excess CO₂ by an outcrop-diffusion model of the ocean. *J. Geophys. Res.*, **88**, 3599-3608.
- Siegenthaler, U. (1989). Carbon-14 in the oceans. In: P. Fritz and J. Ch. Fontes (eds.). *Handbook of environmental isotope geochemistry*, vol. 3. Elsevier, 75-137.
- Sterl, A., and Kattenberg, A. (1994). Embedding a mixed layer model into an ocean general circulation model of the Atlantic: the importance of surface mixing for heat flux and temperature. *J. Geophys. Res.*, **99**, 14139-14157.
- Stocker, T.F., Broecker, W.S., and Wright, D.G. (1994). Carbon uptake experiments with a zonally-averaged global ocean circulation model. *Tellus*, **46B**, 103-122.

Suess, H.E. (1955). Radiocarbon concentration in modern wood. *Science*, 122, 415-417.

Tans, P.P., Fung, I.Y. and Takahashi, T. (1990). Observational constraints on the global atmospheric CO₂ budget. *Science*, 247, 1431-1438.

Taylor, N.K. (1995). Seasonal uptake of anthropogenic CO₂ in an ocean general circulation model. *Tellus*, 47B, 145-169.

Thomas, F., Perigaud, C., Merlivat, L. and Minster, J.F. (1988). World scale monthly mapping of the CO₂ ocean-atmosphere gas transfer coefficient. *Philos. Trans. R. Soc. London Ser. A*, 325, 71-83.

Toggweiler, J.R., Dixon, K., and Bryan, K. (1989a). Simulations of radiocarbon in a coarse-resolution, world ocean model.

1. Steady state, pre-bomb distributions. *J. Geophys. Res.*, 94, 8217-8242

Toggweiler, J.R., Dixon, K., and Bryan, K. (1989b). Simulations of radiocarbon in a coarse-resolution, world ocean model.

2. Distributions of bomb-produced carbon 14. *J. Geophys. Res.*, 94, 8243-8264.

Wallace, D.W.R. (1985). Monitoring global ocean carbon inventories. OOSDP Background Report No. 5. Ocean Observing System Development Panel, Texas A&M University, College Station, TX., USA. 54pp.

Wanninkhof, R. (1992). Relationship between wind speed and gas exchange over the ocean. *J. Geophys. Res.*, 97, 7373-7382.

Warner, M.J. and Weiss, R.F. (1985). Solubilities of chlorofluorocarbons 11 and 12 in water and seawater. *Deep-sea Res.*, 32, 1485-1497.

TABLES

TABLE 1 : Model Vertical Spacing and Global Mean Potential Temperatures and Salinities Versus Observed Values

Level	Depth of	Depth of	Temperature			Salinity		
	level bottom	mid-point	Model	Obs	Difference	Model	Obs	Difference
	(m)	(m)	(°C)			(psu)		
1	10.0	5.0	18.11	17.99	0.12	34.58	34.64	-0.06
2	20.0	15.0	18.11	17.87	0.24	34.58	34.69	-0.11
3	30.0	25.0	18.06	17.68	0.38	34.60	34.75	-0.15
4	40.2	35.1	17.93	17.38	0.55	34.62	34.80	-0.18
5	55.5	47.8	17.62	16.93	0.69	34.65	34.85	-0.20
6	78.5	67.0	17.23	16.36	0.87	34.82	34.96	-0.14
7	113.0	95.7	16.31	15.21	1.10	34.89	35.01	-0.12
8	164.8	138.9	14.91	13.60	1.31	34.95	35.03	-0.08
9	242.6	203.7	13.18	11.72	1.46	34.95	34.98	-0.03
10	359.4	301.0	11.27	9.83	1.43	34.83	34.87	-0.04
11	534.7	447.0	9.38	7.88	1.50	34.71	34.73	-0.02
12	797.9	666.3	7.62	5.89	1.74	34.65	34.62	0.03
13	1193.2	995.5	6.11	4.14	1.97	34.68	34.61	0.07
14	1808.5	1500.8	4.67	2.82	1.85	34.70	34.68	0.02
15	2423.8	2116.1	4.12	2.06	2.06	34.75	34.73	0.02
16	3039.1	2731.3	3.79	1.63	2.16	34.75	34.74	0.01
17	3654.4	3346.6	3.62	1.32	2.30	34.75	34.74	0.01
18	4269.7	3961.9	3.49	1.06	2.43	34.75	34.73	0.02
19	4885.0	4577.1	3.29	0.90	2.39	34.72	34.72	0.00
20	5500.3	5192.4	3.24	1.02	2.22	34.71	34.72	-0.01

TABLE 2 : Regional inventory of excess CO₂. Comparison of model estimates for 1980 with observationally based estimates from Chen (1993)

<u>REGION</u>	<u>EXCESS CARBON (GtC)</u>	
	Model Estimate	Observed Estimate
Greenland and Norwegian Seas (65N to 80 N)	0.81	0.85±0.2
North Atlantic (0 to 65N)	17.9	21.5±4.5
South Atlantic	15.7	12.0±2.5
Total Atlantic	34.4	34.4±7.0
Bering Sea	0.01	0.19±0.15
North Pacific (excluding Bering Sea)	10.3	14.5±4.0
South Pacific	25.5	16.6±4.0
Total Pacific	35.8	31.3±6.0
Indian Ocean	19.0	16.6±3.0
<hr/>		
Total	93.1	82.3±16.0

TABLE 3 : Bomb radiocarbon inventory (10^9 atoms cm^{-2}) at the time of GEOSECS. Comparison of model results against observations and previously published models.

ATLANTIC (1972)

	45N-80N	15N-45N	15S-15N	40S-15S
Observed	13.8	13.2	3.5	9.5
HC Model - Variable Gas Exchange	10.0	7.7	3.5	7.2
HC Model - Fixed Gas Exchange	9.7	10.7	5.9	9.0
Stocker <i>et al</i> (1994) experiment A	11.5	6.2	4.2	7.0
Toggweiler <i>et al</i> (1989) experiment P	11.0	7.1	3.8	8.4

PACIFIC (1974)

	45N-80N	15N-45N	15S-15N	40S-15S
Observed	5.9	9.3	5.7	11.0
HC Model - Variable Gas Exchange	5.7	8.6	3.8	8.0
HC Model - Fixed Gas Exchange	5.7	10.9	6.1	10.7
Stocker <i>et al</i> (1994) experiment A	7.9	7.7	4.8	7.4
Toggweiler <i>et al</i> (1989) experiment P	4.6	8.5	4.4	8.6

INDIAN (1978)

	40S-20N
Observed	8.5
HC Model - Variable Gas Exchange	6.5
HC Model - Fixed Gas Exchange	8.9
Stocker <i>et al</i> (1994) experiment A	6.4
Toggweiler <i>et al</i> (1989) experiment P	8.6

SOUTHERN OCEAN (1974)

	70S-40S
Observed	4.4
HC Model - Variable Gas Exchange	7.0
HC Model - Fixed Gas Exchange	7.1
Stocker <i>et al</i> (1994) experiment A	8.2
Toggweiler <i>et al</i> (1989) experiment P	4.6

GLOBAL INVENTORY (10^{28} atoms) (1975)

Observed	2.9
HC Model - Variable Gas Exchange	2.5
HC Model - Fixed Gas Exchange	3.2
Stocker <i>et al</i> (1994) experiment A	2.6
Toggweiler <i>et al</i> (1989) experiment P	2.4

TABLE 4 : Bomb radiocarbon penetration depths (km) at the time of GEOSECS. Comparison of model results against observations and previously published models.

ATLANTIC (1972)

	45N-80N	15N-45N	15S-15N	40S-15S
Observed	0.80	0.40	0.18	0.38
HC Model - Variable Gas Exchange	0.68	0.32	0.17	0.31
HC Model - Fixed Gas Exchange	0.65	0.31	0.15	0.29
Stocker <i>et al</i> (1994) experiment A	0.61	0.20	0.18	0.24

PACIFIC (1974)

	45N-80N	15N-45N	15S-15N	40S-15S
Observed	0.18	0.34	0.25	0.35
HC Model - Variable Gas Exchange	0.21	0.32	0.20	0.33
HC Model - Fixed Gas Exchange	0.21	0.30	0.19	0.31
Stocker <i>et al</i> (1994) experiment A	0.75	0.25	0.20	0.25

INDIAN (1978)

	40S-20N
Observed	0.32
HC Model - Variable Gas Exchange	0.29
HC Model - Fixed Gas Exchange	0.27
Stocker <i>et al</i> (1994) experiment A	0.23

SOUTHERN OCEAN (1974)

	70S-40S
Observed	0.33
HC Model - Variable Gas Exchange	0.57
HC Model - Fixed Gas Exchange	0.57
Stocker <i>et al</i> (1994) experiment A	0.57

GLOBAL (1975)

Observed	0.34
HC Model - Variable Gas Exchange	0.37
HC Model - Fixed Gas Exchange	0.36
Stocker <i>et al</i> (1994) experiment A	0.29

Figure Captions

Figure 1. The atmospheric $\Delta^{14}\text{C}$ (‰) values used as a boundary condition for the model simulations of bomb ^{14}C uptake.

Figure 2. Modelled zonally-averaged latitude-depth sections of potential temperature ($^{\circ}\text{C}$) and salinity (psu) for a) the Pacific, and b) the Atlantic oceans.

Figure 3. Global overturning streamfunction (Sv) at steady-state.

Figure 4. Modelled depths of the mixed layer (m) during a) March, and b) September. Contours are shown at 25, 50, 100, 200, 500 and 1000m. Depths greater than 500m are shaded. The mixed layer realises its maximum extent in the northern and southern hemispheres during these months.

Figure 5. Modelled horizontal currents (cm s^{-1}) at depths of a) 5m, b) 100m, and c) 2100m.

Figure 6. Modelled natural radiocarbon at a) the surface, and latitude-depth sections through b) the Atlantic, and c) the Pacific oceans. All data are from the spatially varying gas exchange run.

Figure 7. Annually-averaged pre-industrial atmosphere-ocean flux of CO_2 ($\text{mole m}^{-2} \text{yr}^{-1}$) from the variable gas exchange run. Positive fluxes, representing net oceanic uptake, are shaded.

Figure 8. Time history of the atmospheric CO_2 concentration (ppmv) used to force the carbon cycle model.

Figure 9. Time-series of the modelled net atmosphere-ocean CO_2 fluxes (GtC yr^{-1}) plotted by region. Positive values represent uptake by the ocean.

Figure 10. Time-series of the modelled net atmosphere-ocean CO_2 fluxes shown as a perturbation from the pre-industrial state. The data for each region are displayed as a fraction of the global excess carbon uptake. (___) $>45^{\circ}\text{S}$, (____) $0-45^{\circ}\text{S}$, (—) $0-45^{\circ}\text{N}$, (.....) N Atlantic $>45^{\circ}\text{N}$, (----) N Pacific $>45^{\circ}\text{N}$.

Figure 11. Spatial distribution of the atmosphere-ocean flux of excess CO_2 ($\text{mole m}^{-2} \text{yr}^{-1}$) in 1990 from the variable gas exchange run. Regions of low uptake (below $0.4 \text{ mole m}^{-2} \text{yr}^{-1}$) are lightly shaded. Regions of high uptake (above $1.6 \text{ mole m}^{-2} \text{yr}^{-1}$) are cross-hatched.

Figure 12. Comparison of global net CO_2 fluxes (GtC yr^{-1}) from runs using fixed (---) and spatially variable (___) gas exchange formulations.

Figure 13. Difference in atmosphere-ocean CO_2 flux ($\text{mole m}^{-2} \text{yr}^{-1}$) between runs using variable and fixed gas exchange formulations. Positive and negative differences in excess of $0.4 \text{ mole m}^{-2} \text{yr}^{-1}$ are shaded.

Figure 14. a) Modelled annual cycle of primary production ($\text{gC m}^{-2} \text{d}^{-1}$) at OWS India in the North-East Atlantic. b) pCO_2 (μatm) at OWS India from runs with (---) and without (___) the biological pump included. The late spring/summer bloom causes a fall in pCO_2 , sustaining values below the ambient atmospheric value throughout the summer and autumn.

Figure 15. IPCC scenarios for future pCO_2 levels stabilising at 450 μatm and 650 μatm used to force the model.

Figure 16. a) Modelled oceanic CO_2 uptake, and b) estimated net emissions (fossil fuel+land-use change+biospheric sources/sinks) required to achieve the targets for atmospheric pCO_2 shown in Figure 15.

Figure 17. Net biospheric sink (___) computed as the residual after oceanic uptake and atmospheric accumulation have been subtracted from fossil fuel emissions. Also shown is the source due to deforestation (.....) (from data supplied to the IPCC by R.A. Houghton), and the implied terrestrial CO_2 fertilisation sink (---).

Figure 18. Optimum fit to the hypothesised terrestrial sink of CO_2 using linear (___), logarithmic (.....) and logistic (----) functions of atmospheric CO_2 concentration. The terrestrial sink, S_{fert} , calculated as the residual from equation (10) is shown by asterisks.

Figure 19. Estimated fossil fuel emissions (GtC yr^{-1}) required to achieve stabilisation at a) 450 μatm , and b) 650 μatm under three different assumptions of the future behaviour of the terrestrial biosphere.

Figure 20. Model bomb radiocarbon inventory ($10^9 \text{ atoms cm}^{-2}$) at the time of GEOSECS. Data are shown for 1972 (Pacific), 1974 (Atlantic), and 1978 (Indian Ocean). Values below $4 \times 10^9 \text{ atoms cm}^{-2}$ and values above $16 \times 10^9 \text{ atoms cm}^{-2}$ are shaded. All data are from the spatially varying gas exchange run.

Figure 21. Profiles of globally averaged potential temperature (a), and salinity (b) from runs with (___) and without (---) the Mediterranean outflow parametrisation, and from the observed Levitus climatology (.....).

Figure 22. Time-history of the dry air mole fraction of CFC-11 in the atmosphere since 1950. This function was used as the atmospheric boundary condition for the simulation of CFC-11 uptake. The southern hemisphere history (----) lags the northern hemisphere history (___) slightly.

Figure 23. a) Observed distribution of CFC-11 along the Greenwich Meridian during late 1983 (from Warner and Weiss, 1992). b) Model distribution along the same section for December 1983. Contour levels are at 0.015, 0.03, 0.05, 0.1, 0.2, 0.4, 0.8, 1.6 and 3.2 pico-mol kg^{-1} .

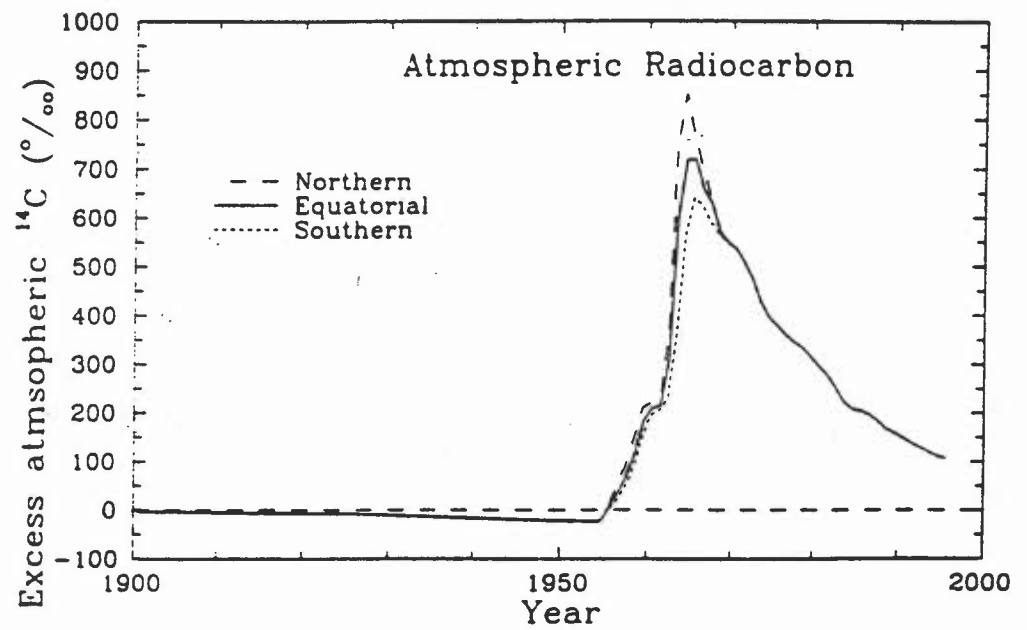


Figure 1. The atmospheric $\Delta^{14}\text{C}$ (‰) values used as a boundary condition for the model simulations of bomb ^{14}C uptake.

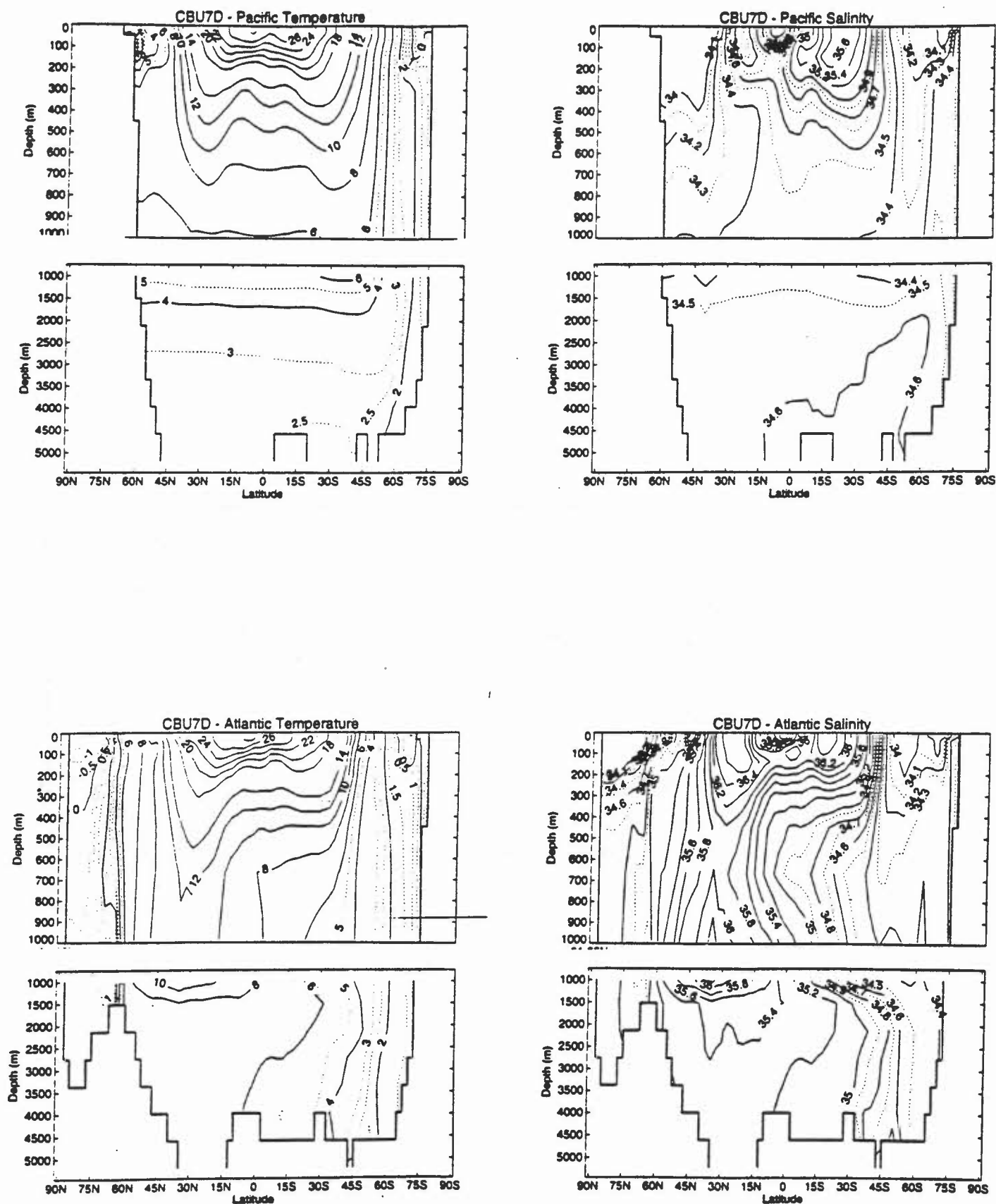


Figure 2. Modelled zonally-averaged latitude-depth sections of potential temperature ($^{\circ}\text{C}$) and salinity (psu) for a) the Pacific, and b) the Atlantic oceans.

Global Meridional Streamfunction

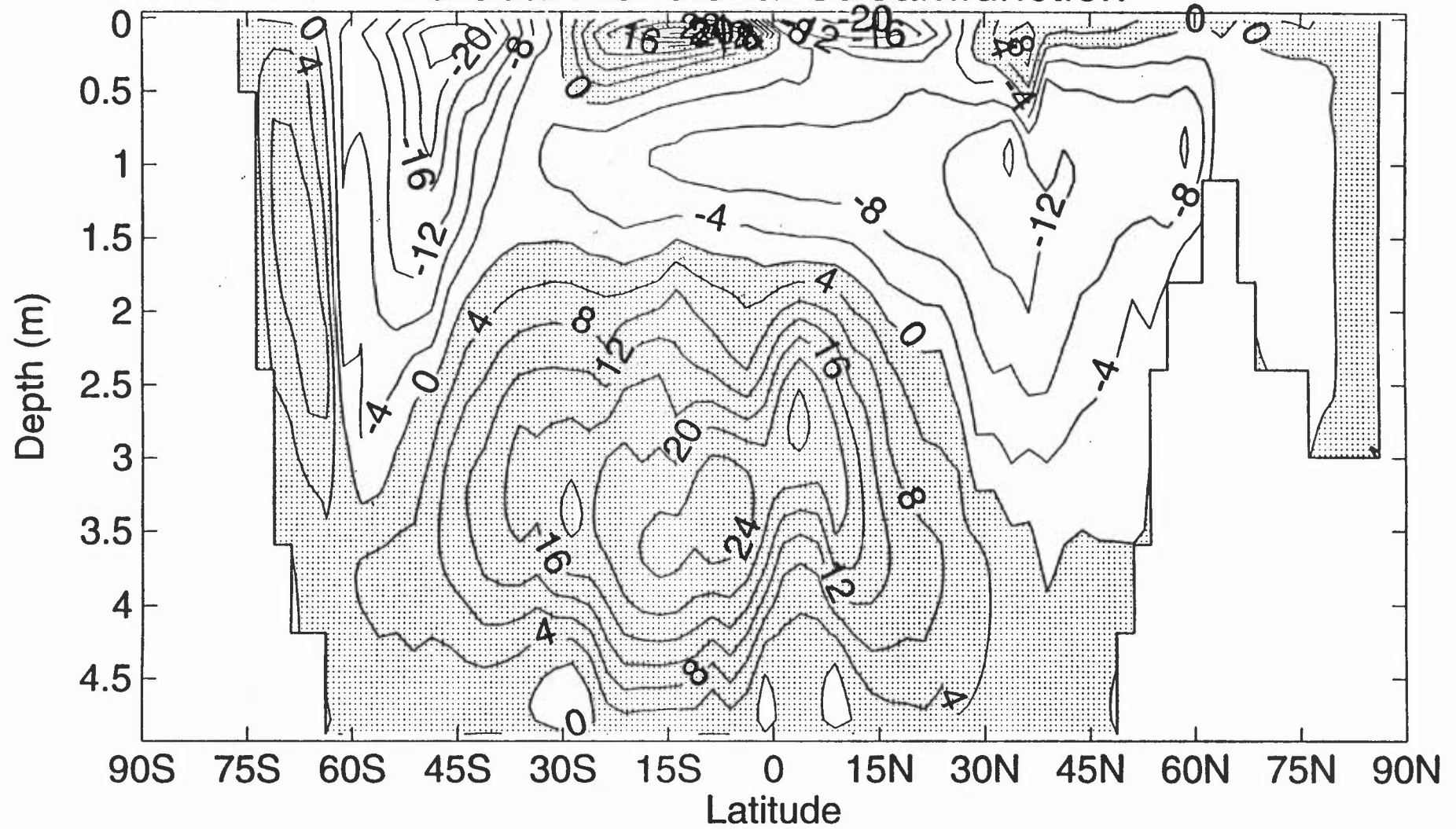


Figure3. Global overturning streamfunction (Sv) at steady-state.

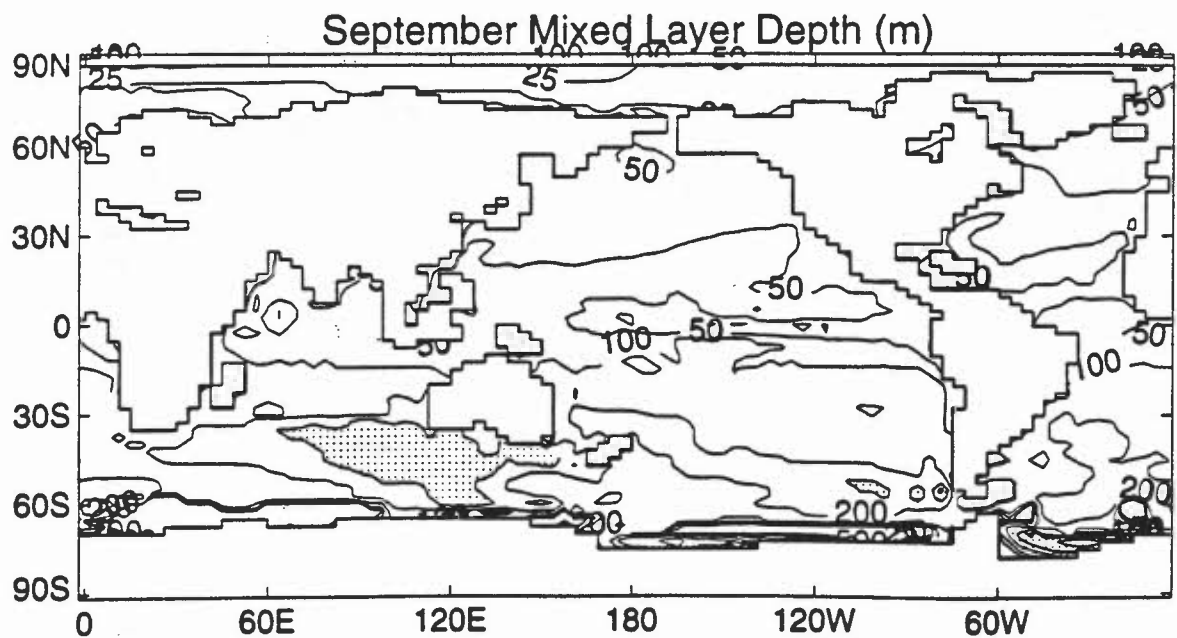
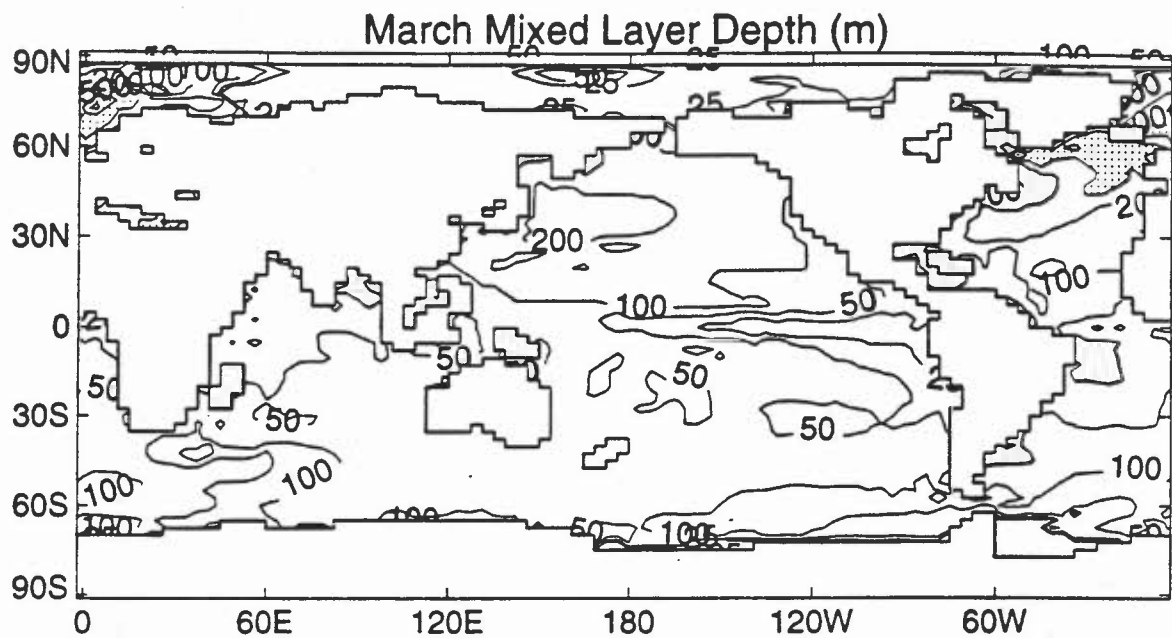


Figure 4. Modelled depths of the mixed layer (m) during a) March, and b) September. Contours are shown at 25, 50, 100, 200, 500 and 1000m. Depths greater than 500m are shaded. The mixed layer realises its maximum extent in the northern and southern hemispheres during these months.

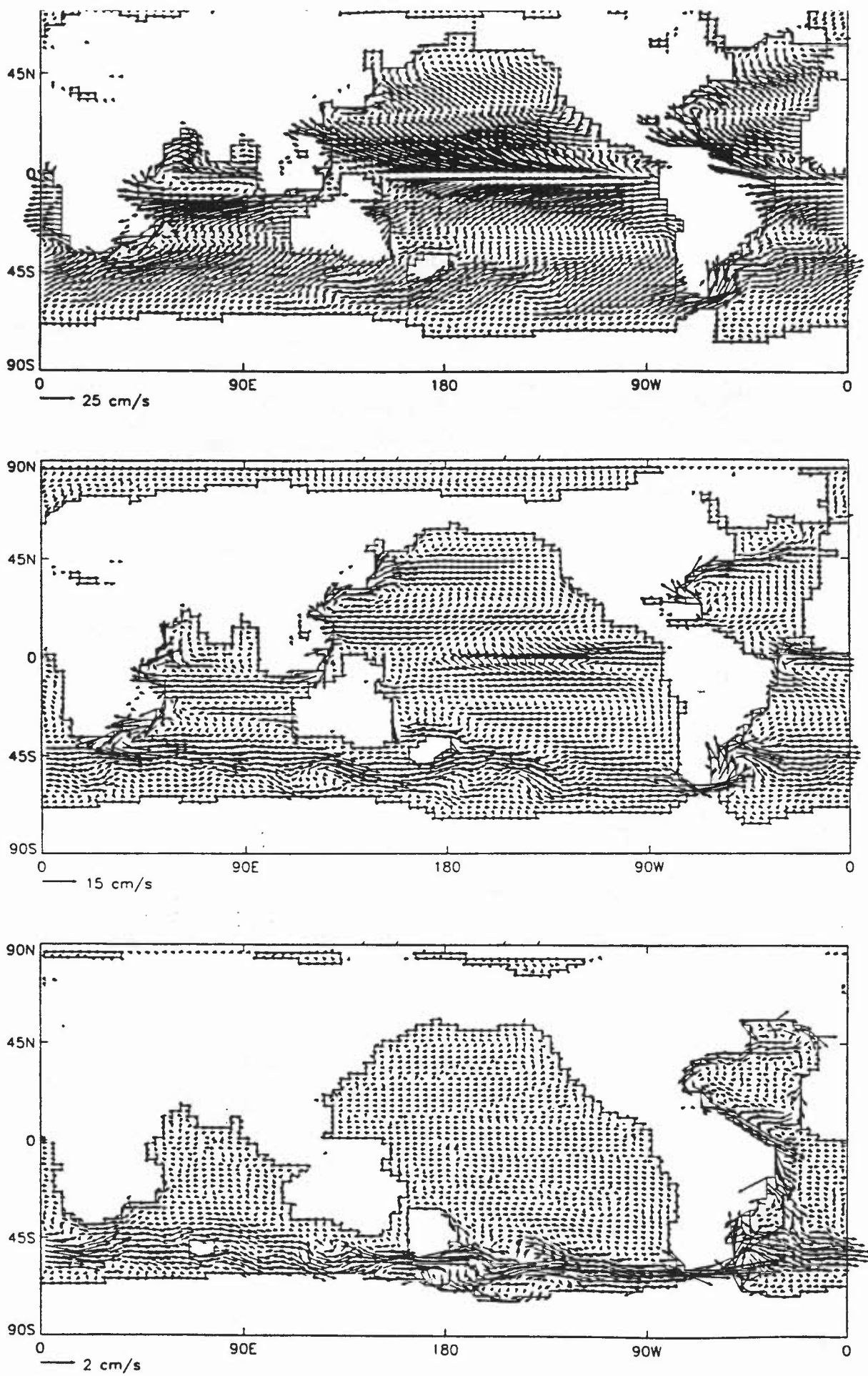


Figure 5. Modelled horizontal currents (cm s^{-1}) at depths of a) 5m, b) 100m, and c) 2100m.

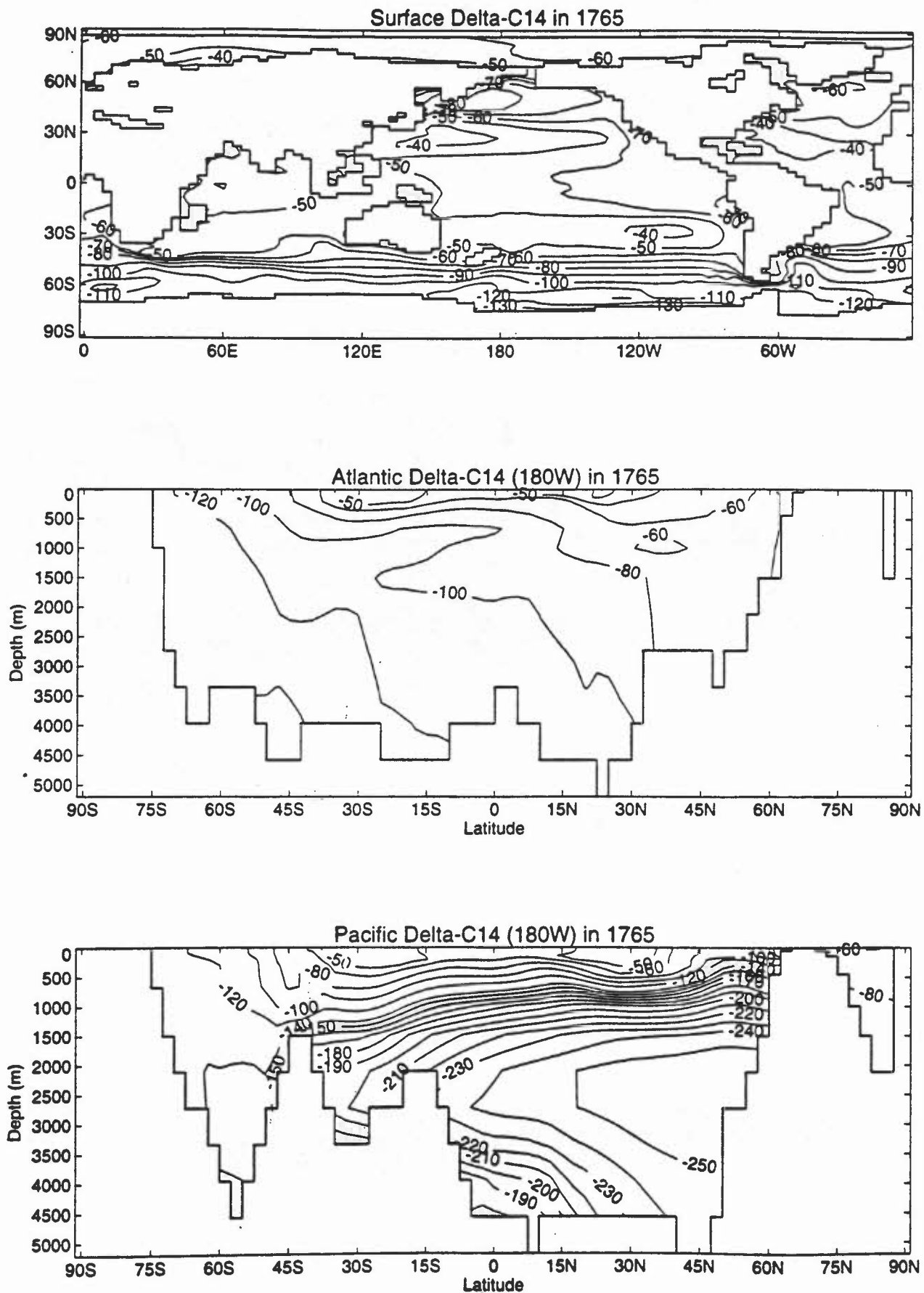


Figure 6. Modelled natural radiocarbon at a) the surface, and latitude-depth sections through b) the Atlantic, and c) the Pacific oceans. All data are from the spatially varying gas exchange run.

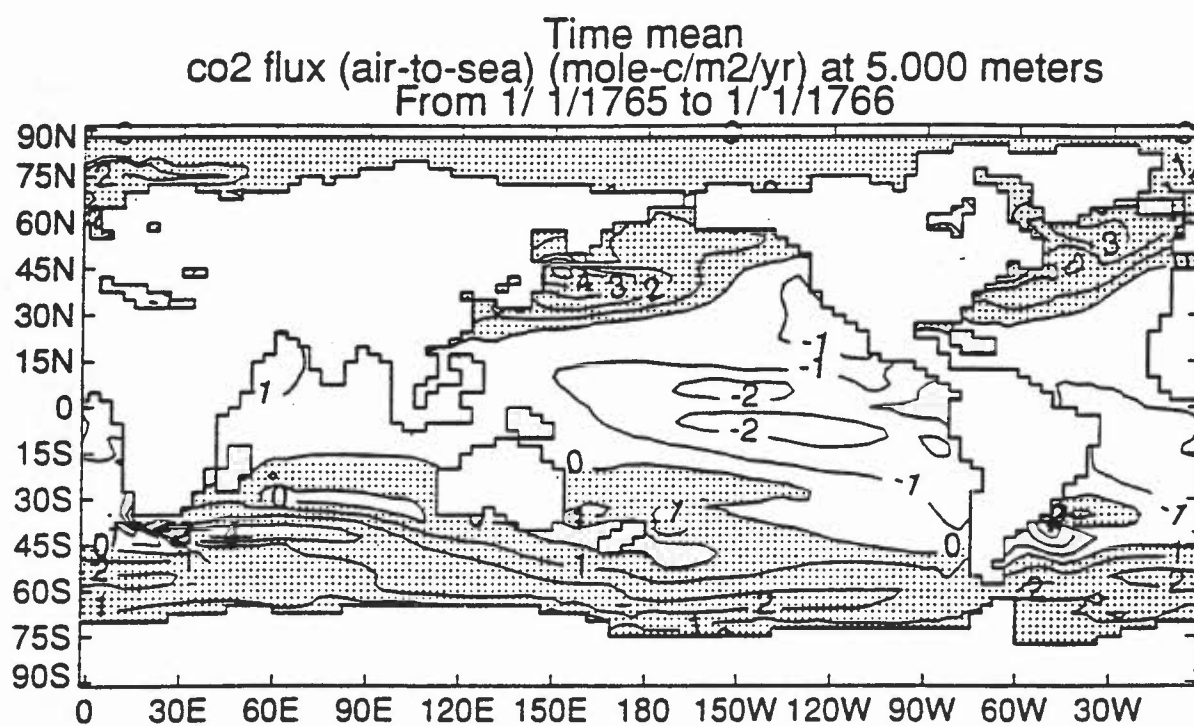


Figure 7. Annually-averaged pre-industrial atmosphere-ocean flux of CO₂ (mole m⁻² yr⁻¹) from the variable gas exchange run. Positive fluxes, representing net oceanic uptake, are shaded.

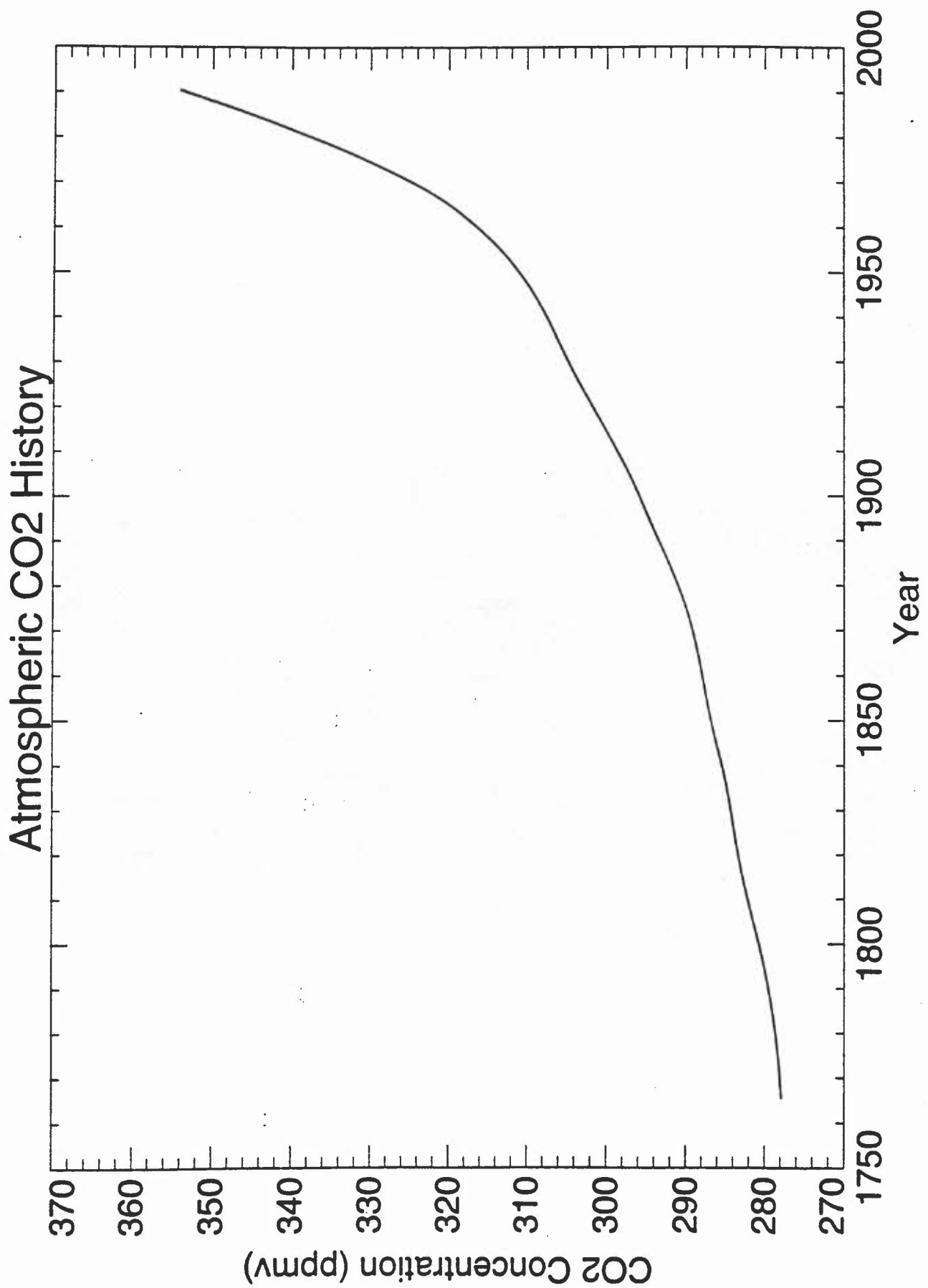


Figure 8. Time history of the atmospheric CO₂ concentration (ppmv) used to force the carbon cycle model.

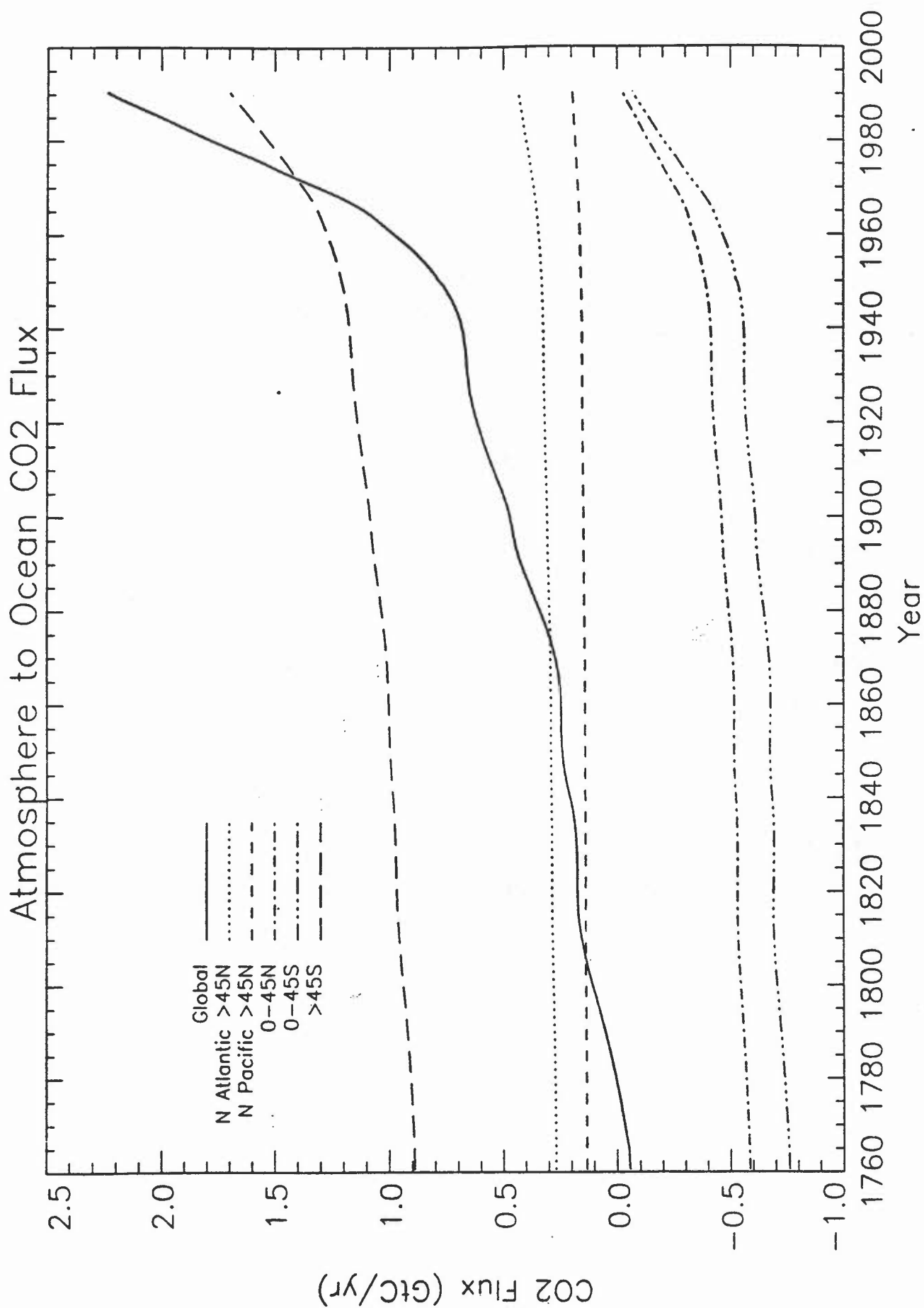


Figure 9. Time-series of the modelled net atmosphere-ocean CO₂ fluxes (GtC yr⁻¹) plotted by region. Positive values represent uptake by the ocean.

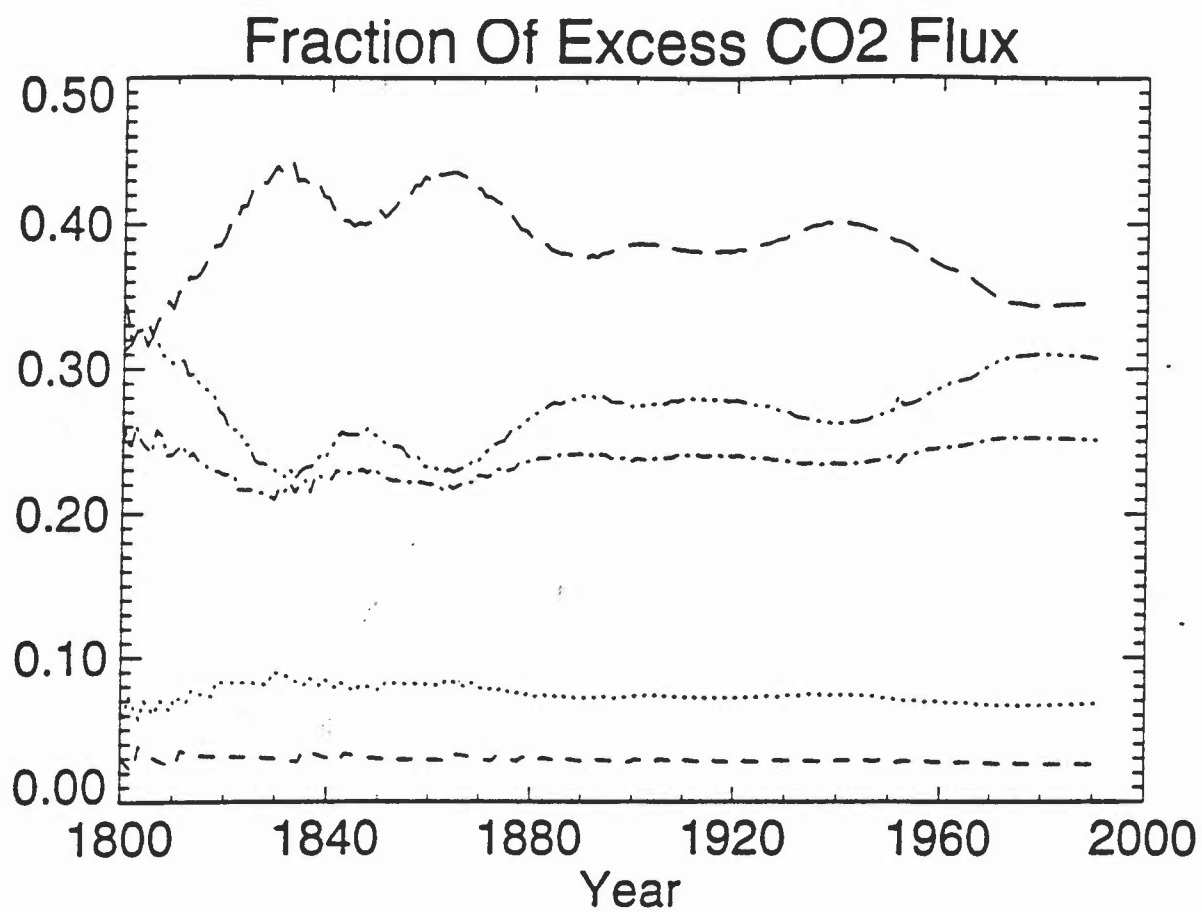


Figure 10. Time-series of the modelled net atmosphere-ocean CO₂ fluxes shown as a perturbation from the pre-industrial state. The data for each region are displayed as a fraction of the global excess carbon uptake. (— —) $>45^{\circ}\text{S}$, (— · —) $0-45^{\circ}\text{S}$, (— —) $0-45^{\circ}\text{N}$, (.....) N Atlantic $>45^{\circ}\text{N}$, (— —) N Pacific $>45^{\circ}\text{N}$.

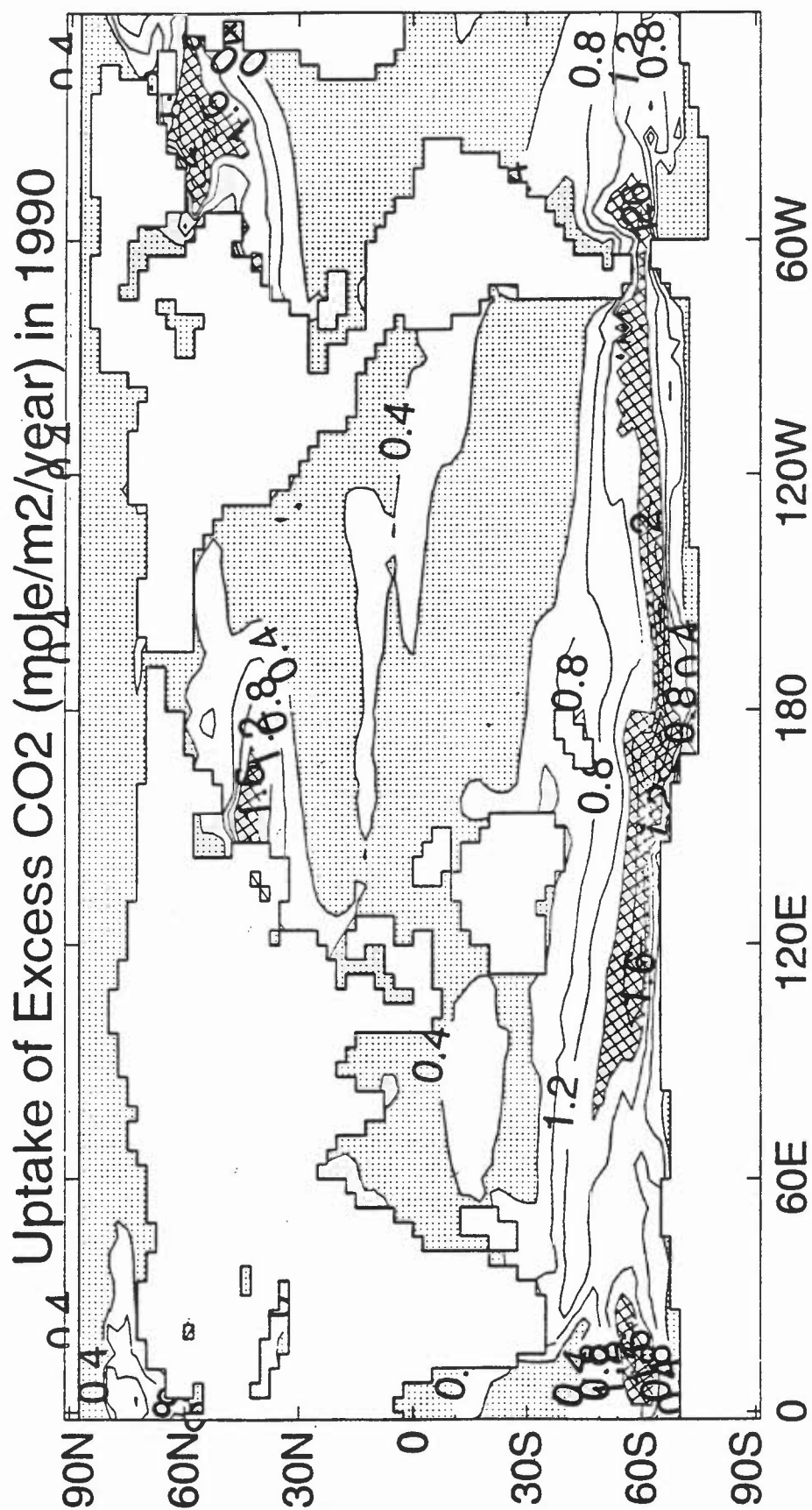


Figure 11. Spatial distribution of the atmosphere-ocean flux of excess CO₂ (mole m⁻² yr⁻¹) in 1990 from the variable gas exchange run. Regions of low uptake (below 0.4 mole m⁻² yr⁻¹) are lightly shaded. Regions of high uptake (above 1.6 mole m⁻² yr⁻¹) are cross-hatched.

Atmosphere to Ocean CO2 Flux

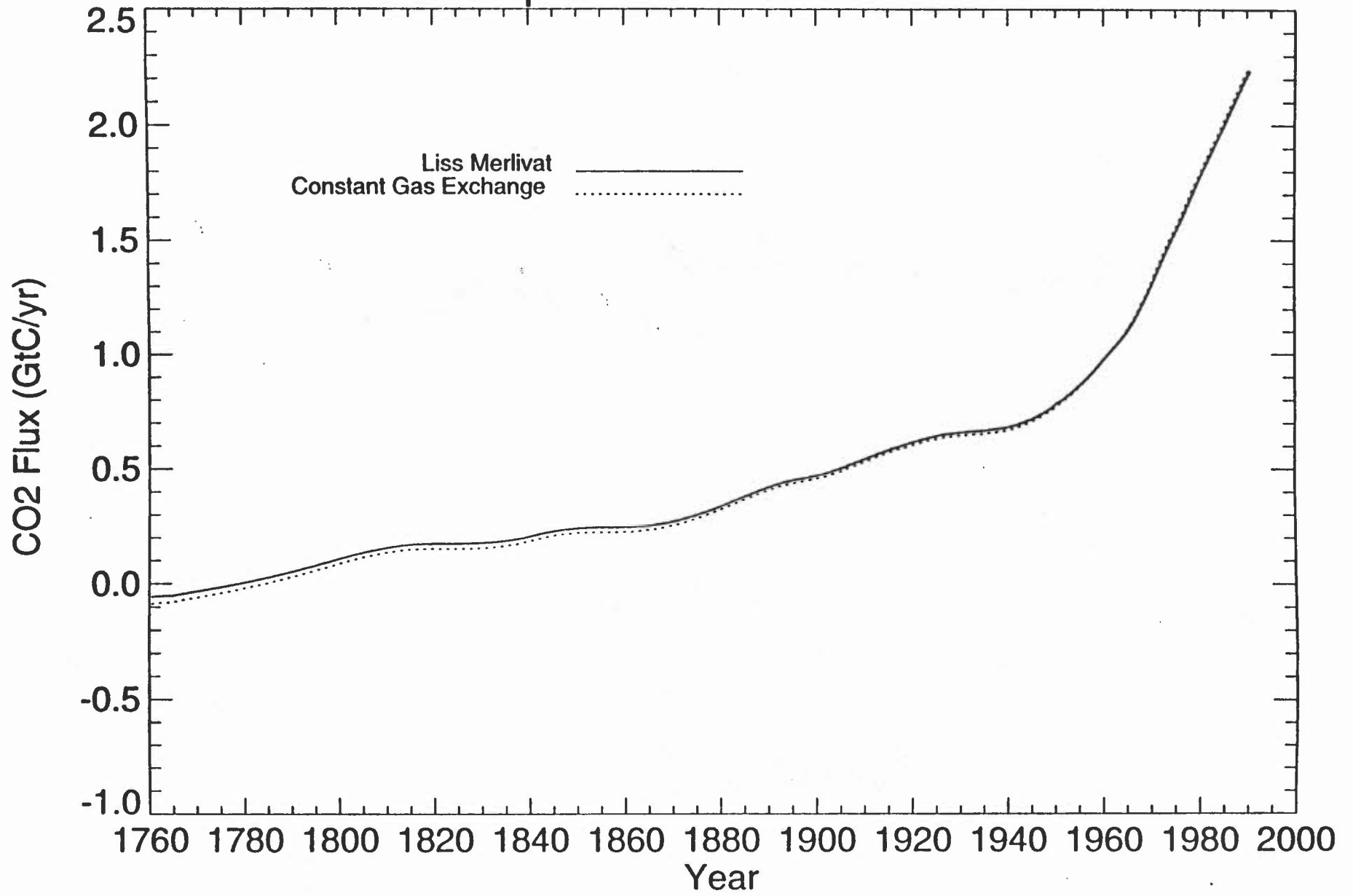


Figure 12. Comparison of global net CO2 fluxes (GtC yr⁻¹) from runs using fixed (---) and spatially variable (—) gas exchange formulations.

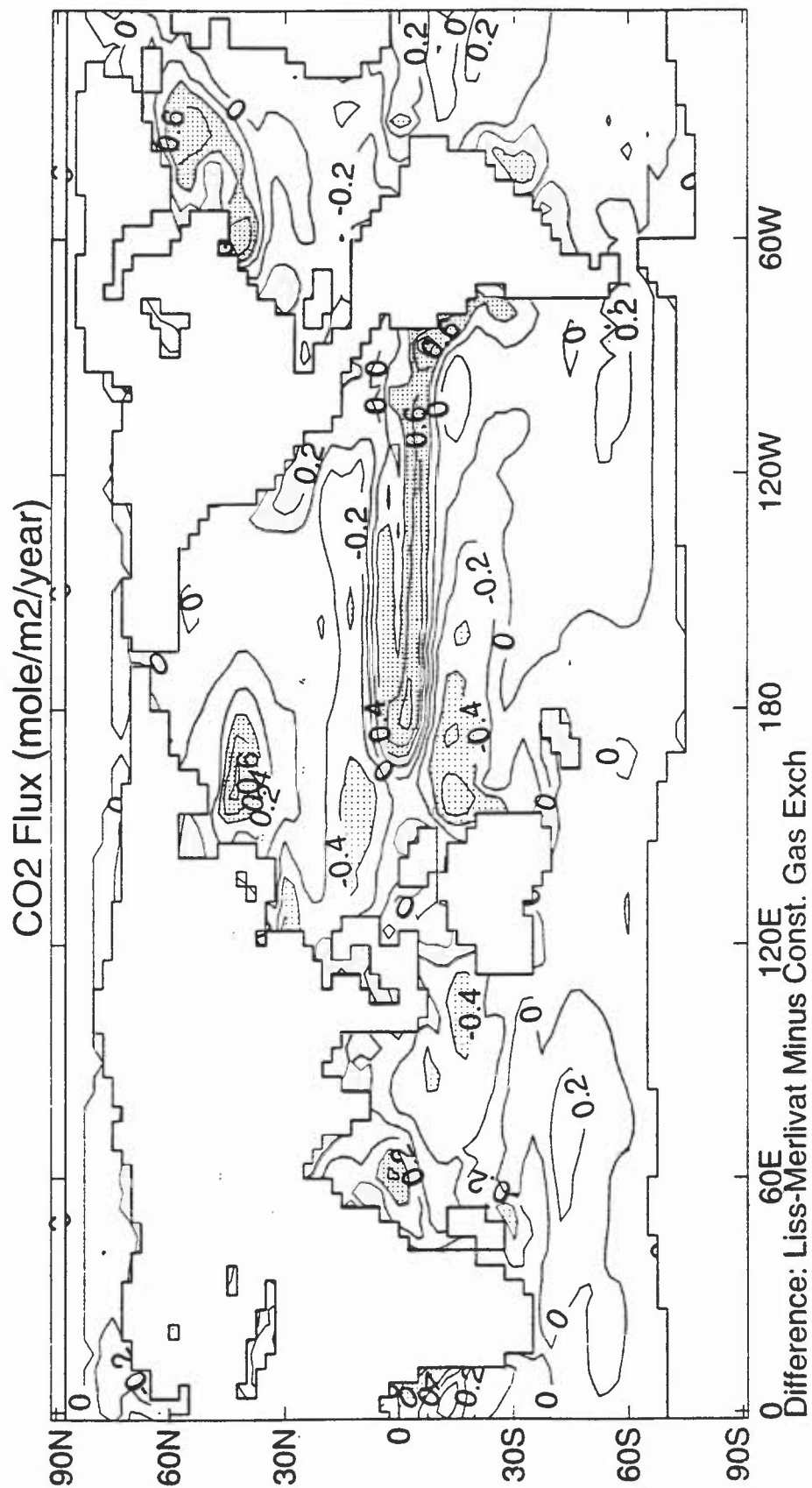


Figure 13. Difference in atmosphere-ocean CO₂ flux (mole m⁻² yr⁻¹) between runs using variable and fixed gas exchange formulations. Positive and negative differences in excess of 0.4 mole m⁻² yr⁻¹ are shaded.

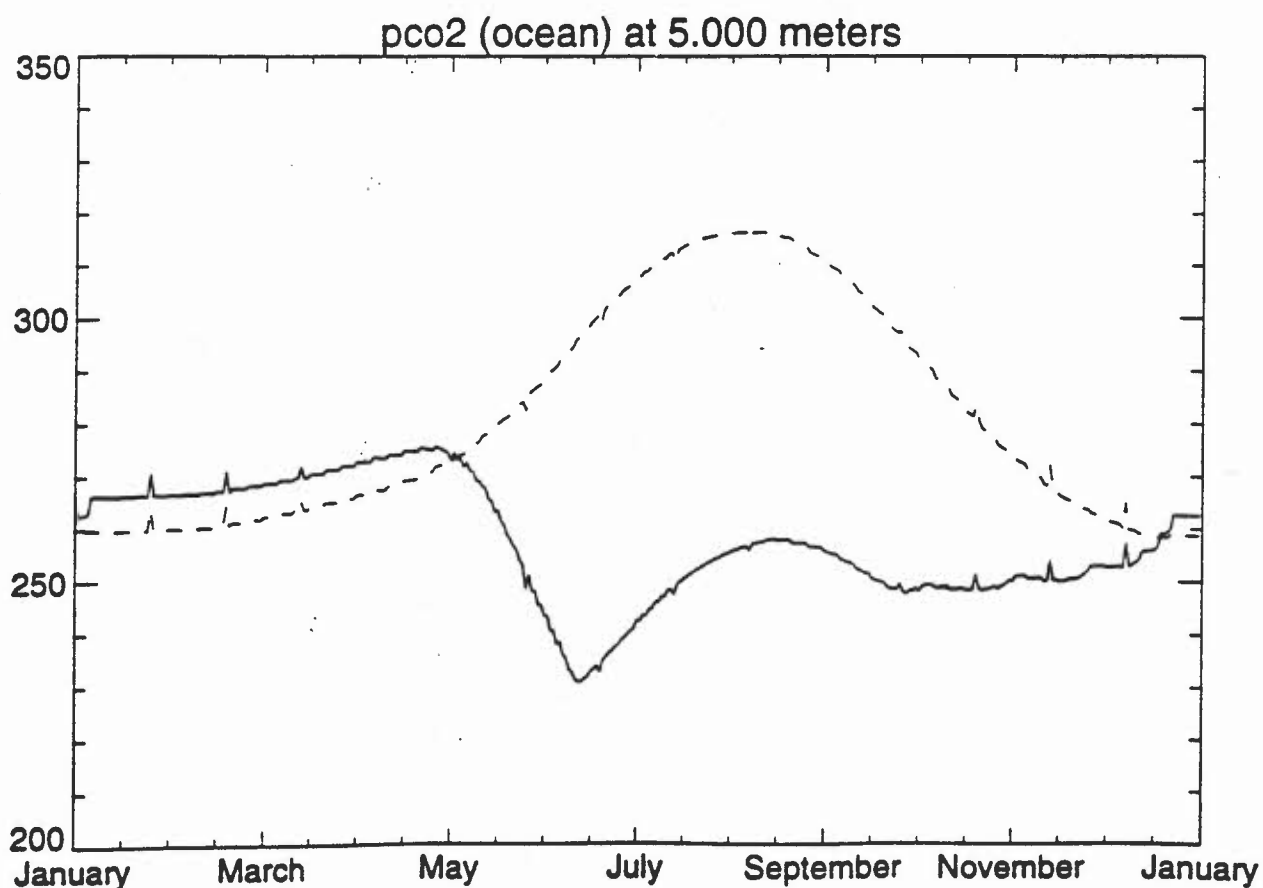
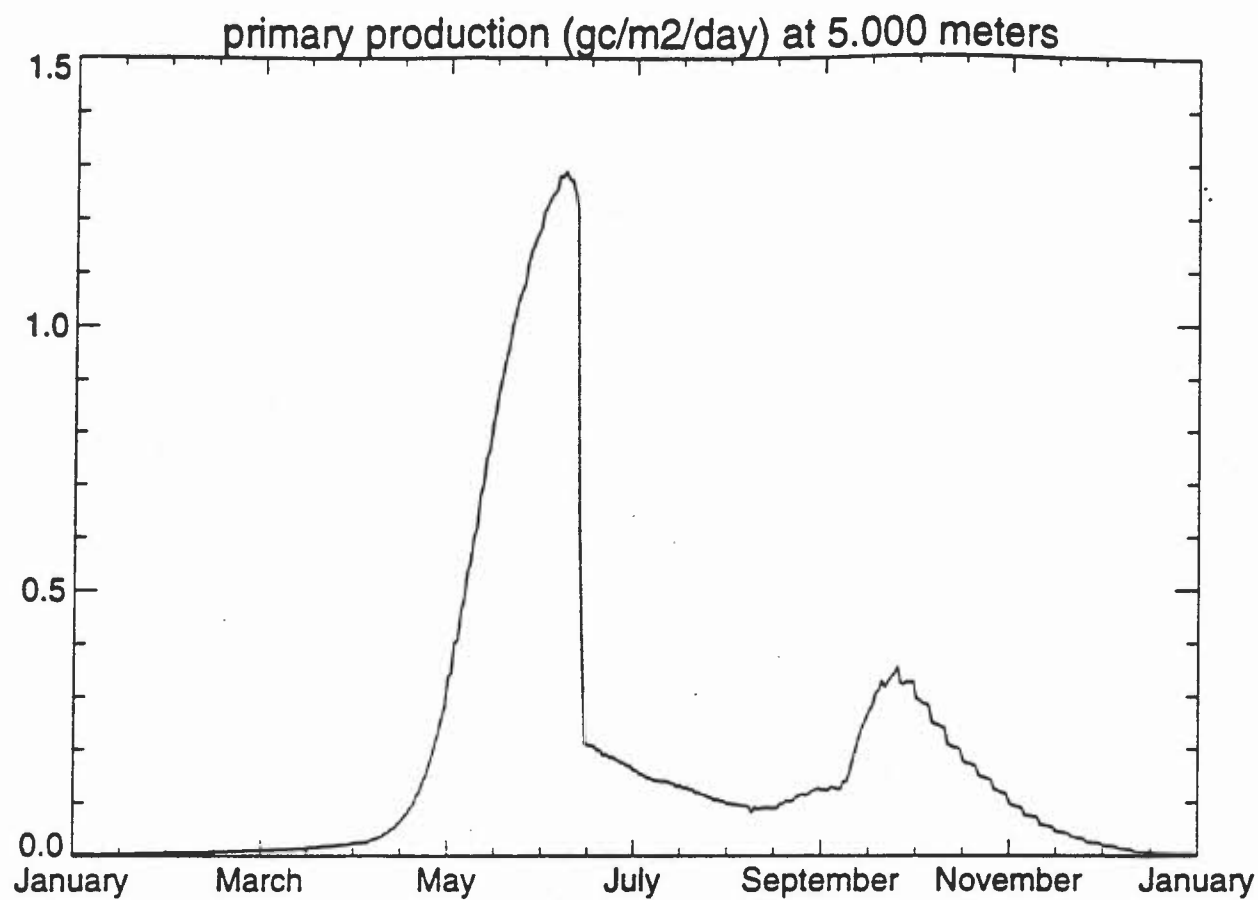


Figure 14. a) Modelled annual cycle of primary production ($\text{gC m}^{-2} \text{d}^{-1}$) at OWS India in the North-East Atlantic. b) pCO_2 (μatm) at OWS India from runs with (---) and without (—) the biological pump included. The late spring/summer bloom causes a fall in pCO_2 , sustaining values below the ambient atmospheric value throughout the summer and autumn.

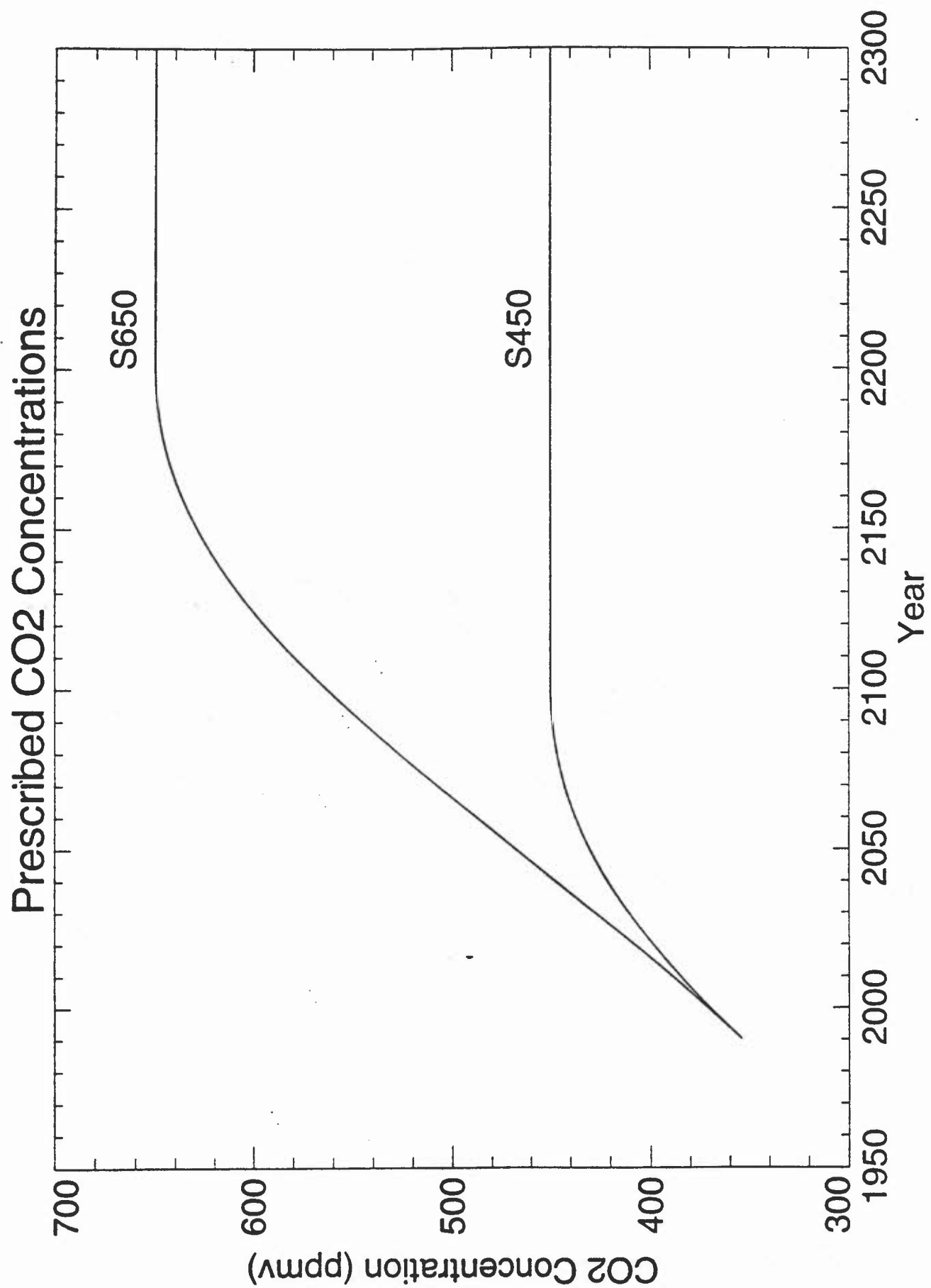


Figure 15. IPCC scenarios for future pCO₂ levels stabilising at 450 μ atm and 650 μ atm used to force the model.

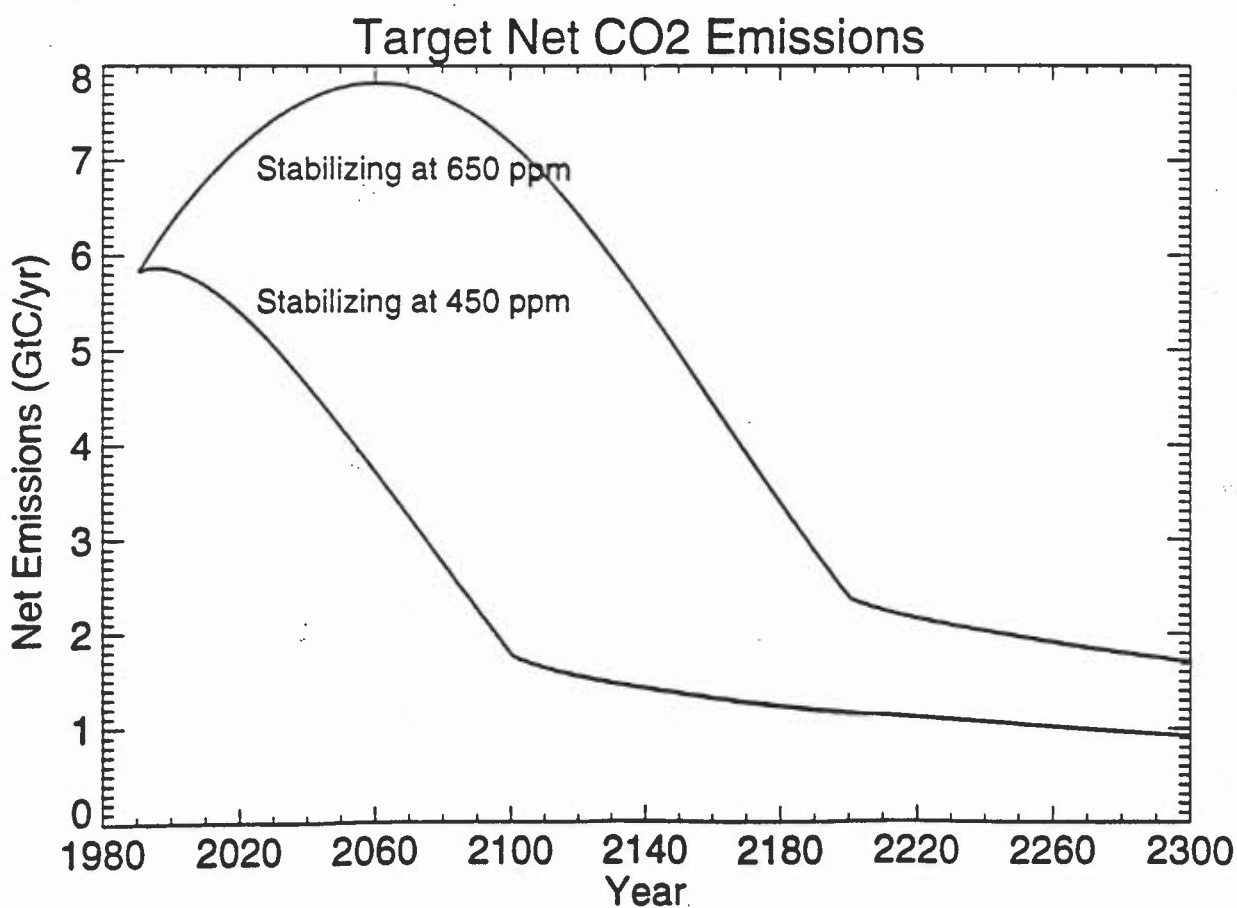
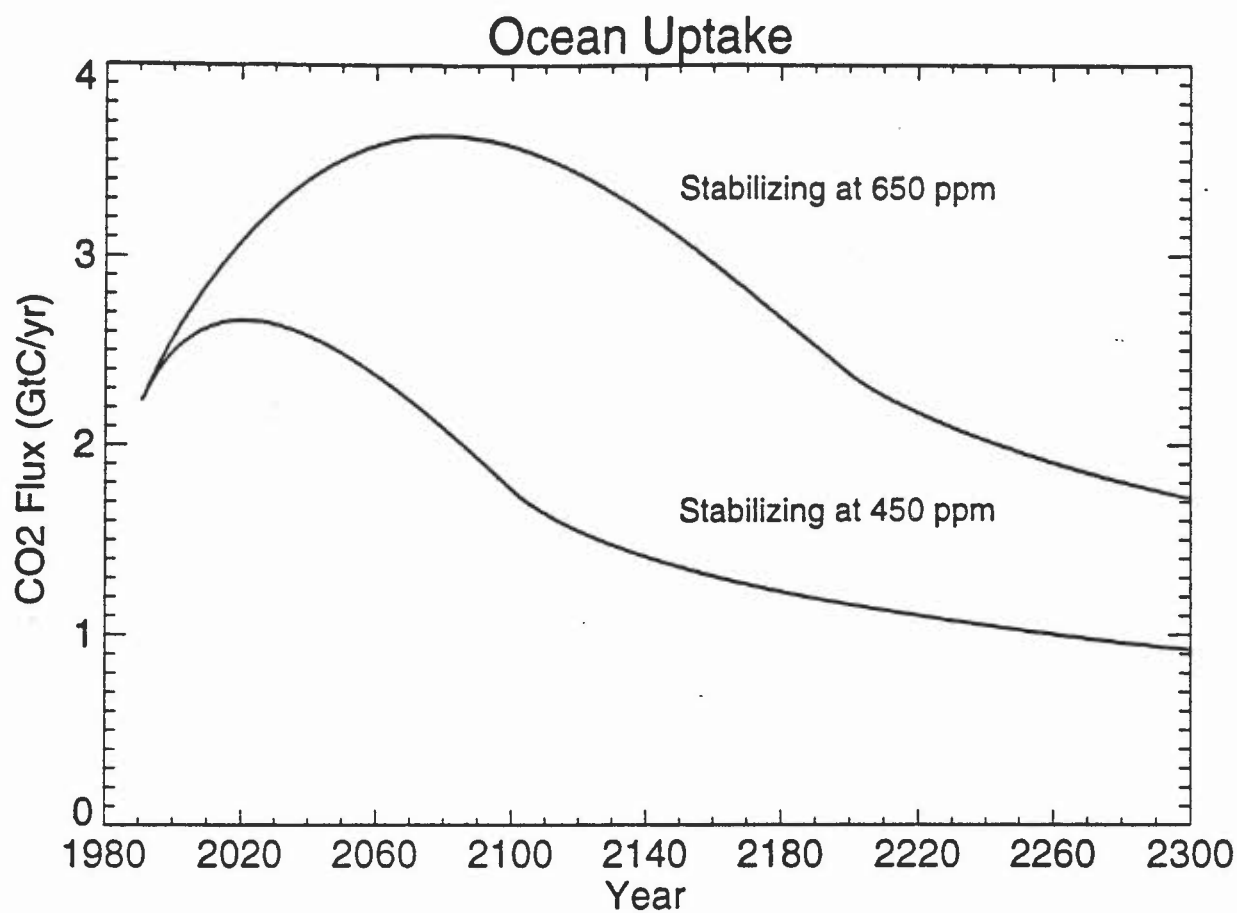


Figure 16. a) Modelled oceanic CO₂ uptake, and b) estimated net emissions (fossil fuel+land-use change+biospheric sources/sinks) required to achieve the targets for atmospheric pCO₂ shown in Figure 15.

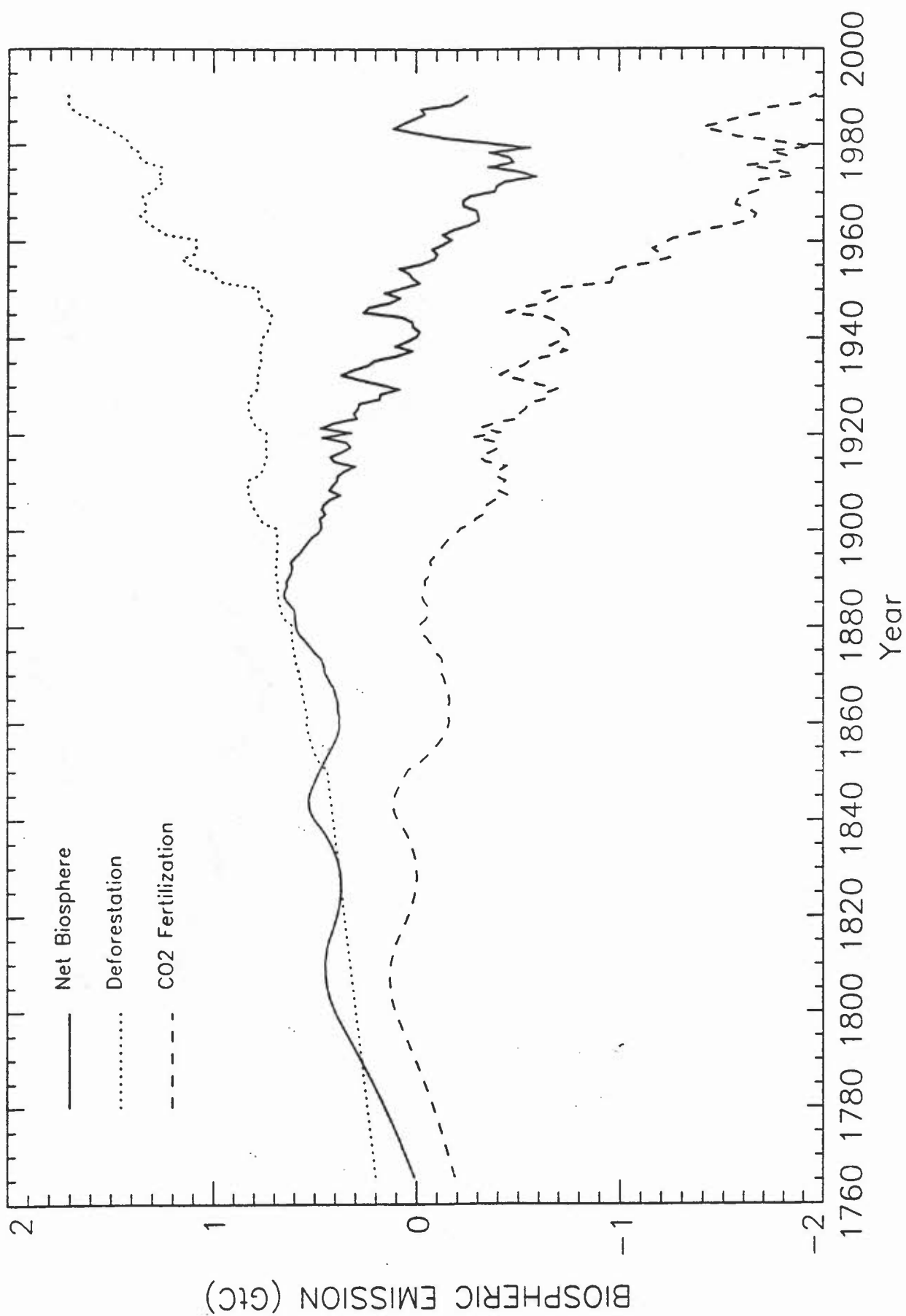


Figure 17. Net biospheric sink (—) computed as the residual after oceanic uptake and atmospheric accumulation have been subtracted from fossil fuel emissions. Also shown is the source due to deforestation (.....) (from data supplied to the IPCC by R.A. Houghton), and the implied terrestrial CO₂ fertilisation sink (- - -).

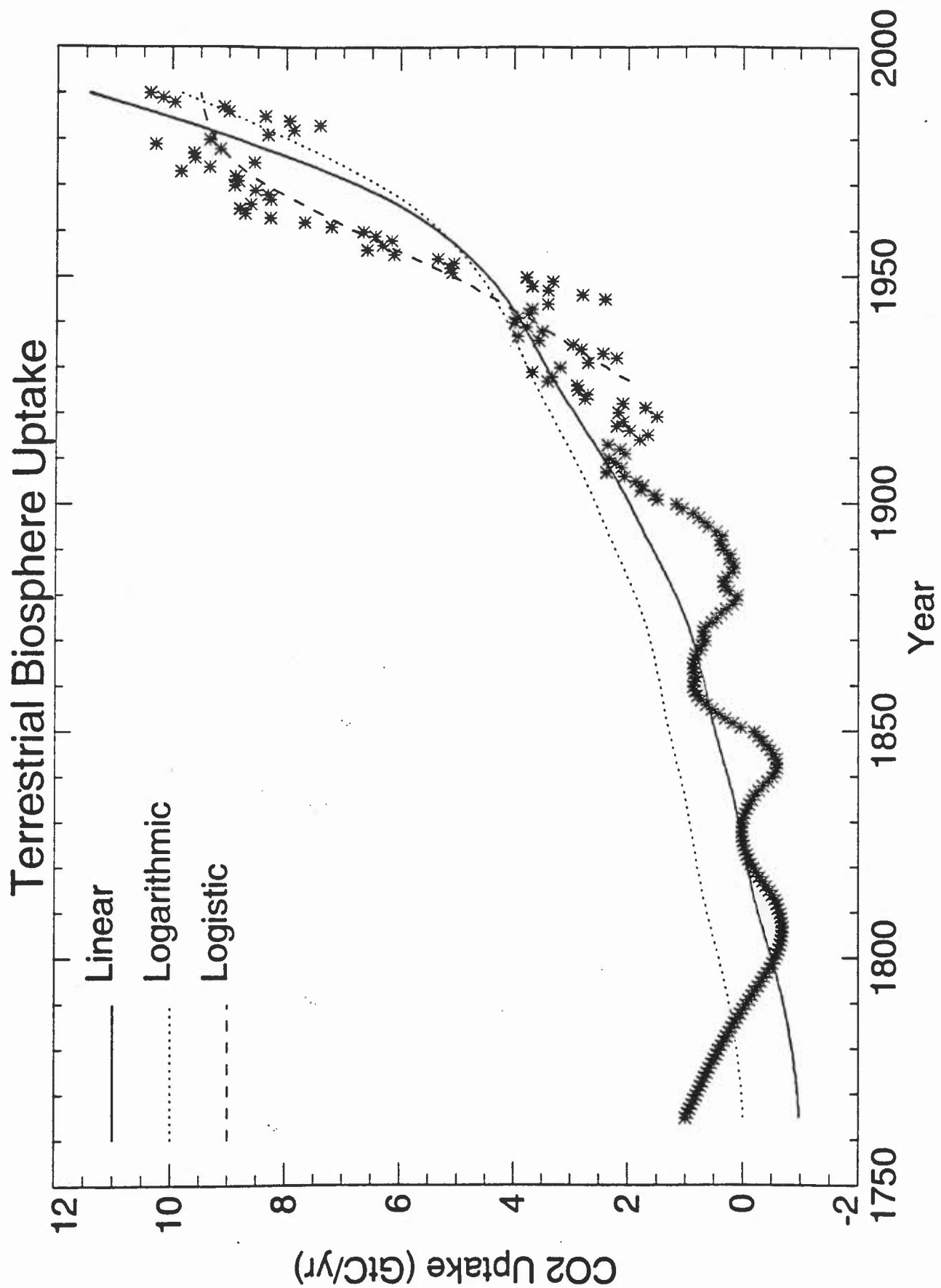


Figure 18. Optimum fit to the hypothesised terrestrial sink of CO₂ using linear (—), logarithmic (....) and logistic (---) functions of atmospheric CO₂ concentration. The terrestrial sink, S_{ter} , calculated as the residual from equation (10) is shown by asterisks.

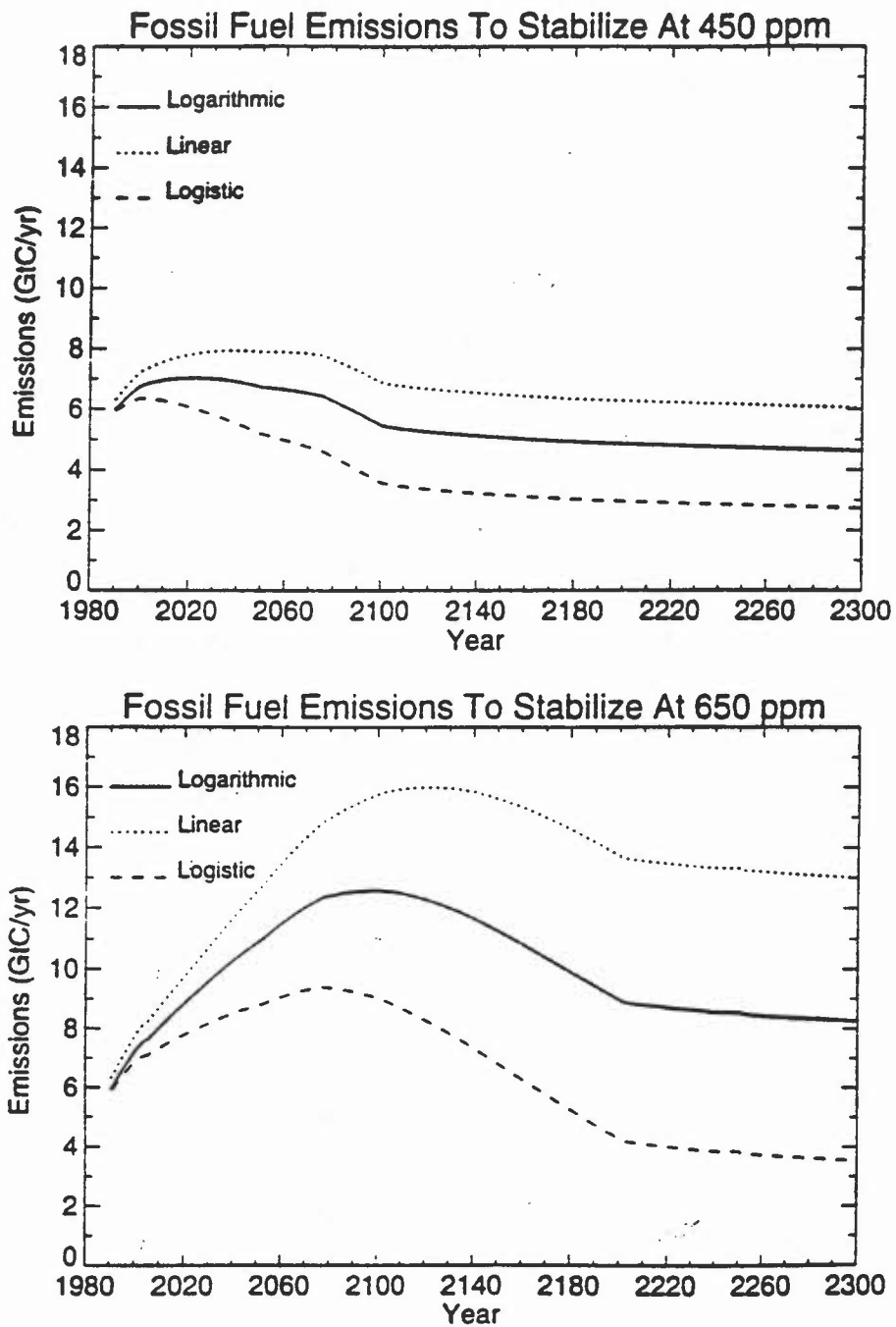


Figure 19. Estimated fossil fuel emissions (GtC yr^{-1}) required to achieve stabilisation at a) $450 \mu\text{atm}$, and b) $650 \mu\text{atm}$ under three different assumptions of the future behaviour of the terrestrial biosphere.

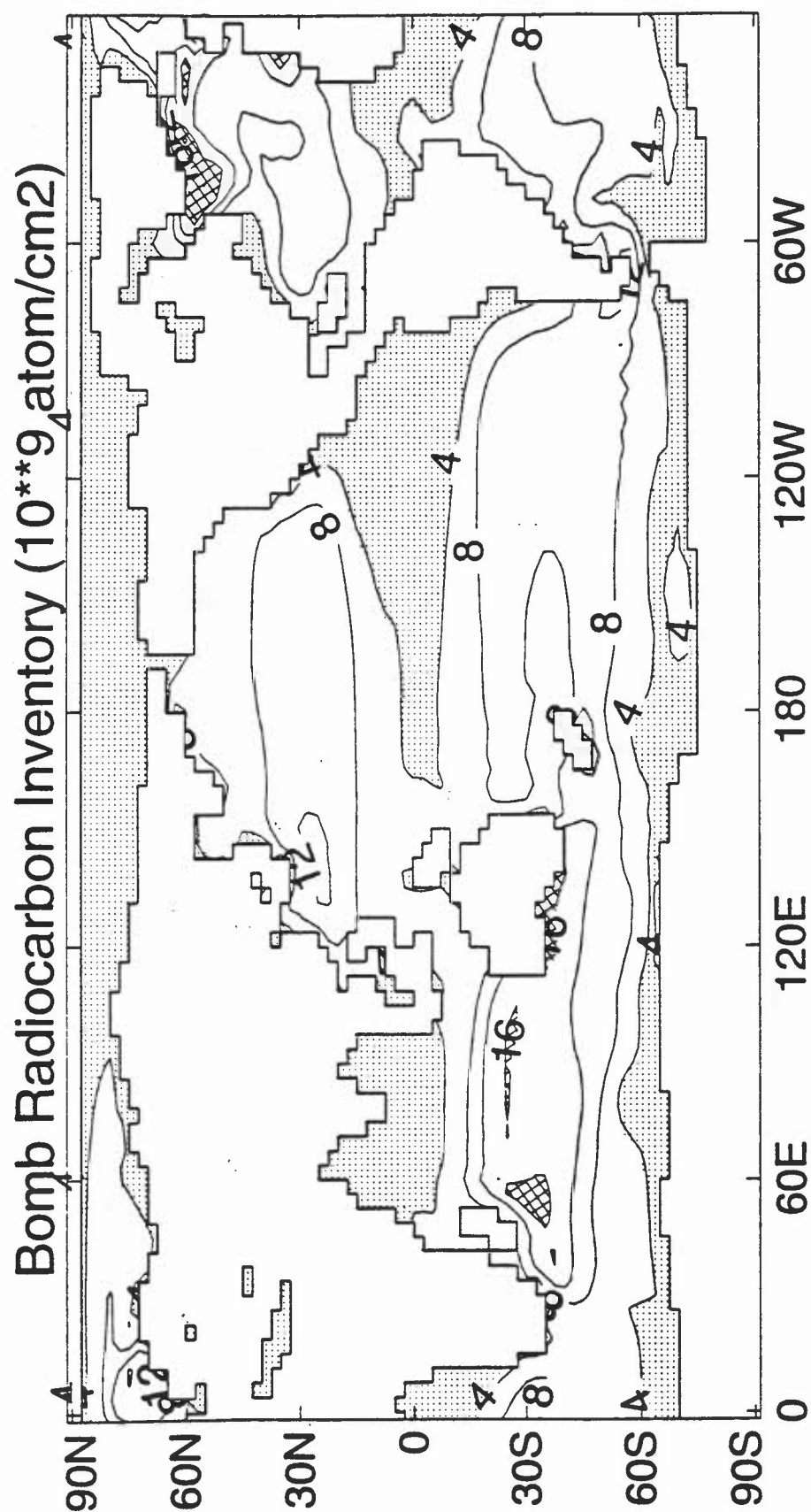


Figure 20. Model bomb radiocarbon inventory (10^9 atoms cm^{-2}) at the time of GEOSECS. Data are shown for 1972 (Pacific), 1974 (Atlantic), and 1978 (Indian Ocean). Values below 4×10^9 atoms cm^{-2} and values above 16×10^9 atoms cm^{-2} are shaded. All data are from the spatially varying gas exchange run.

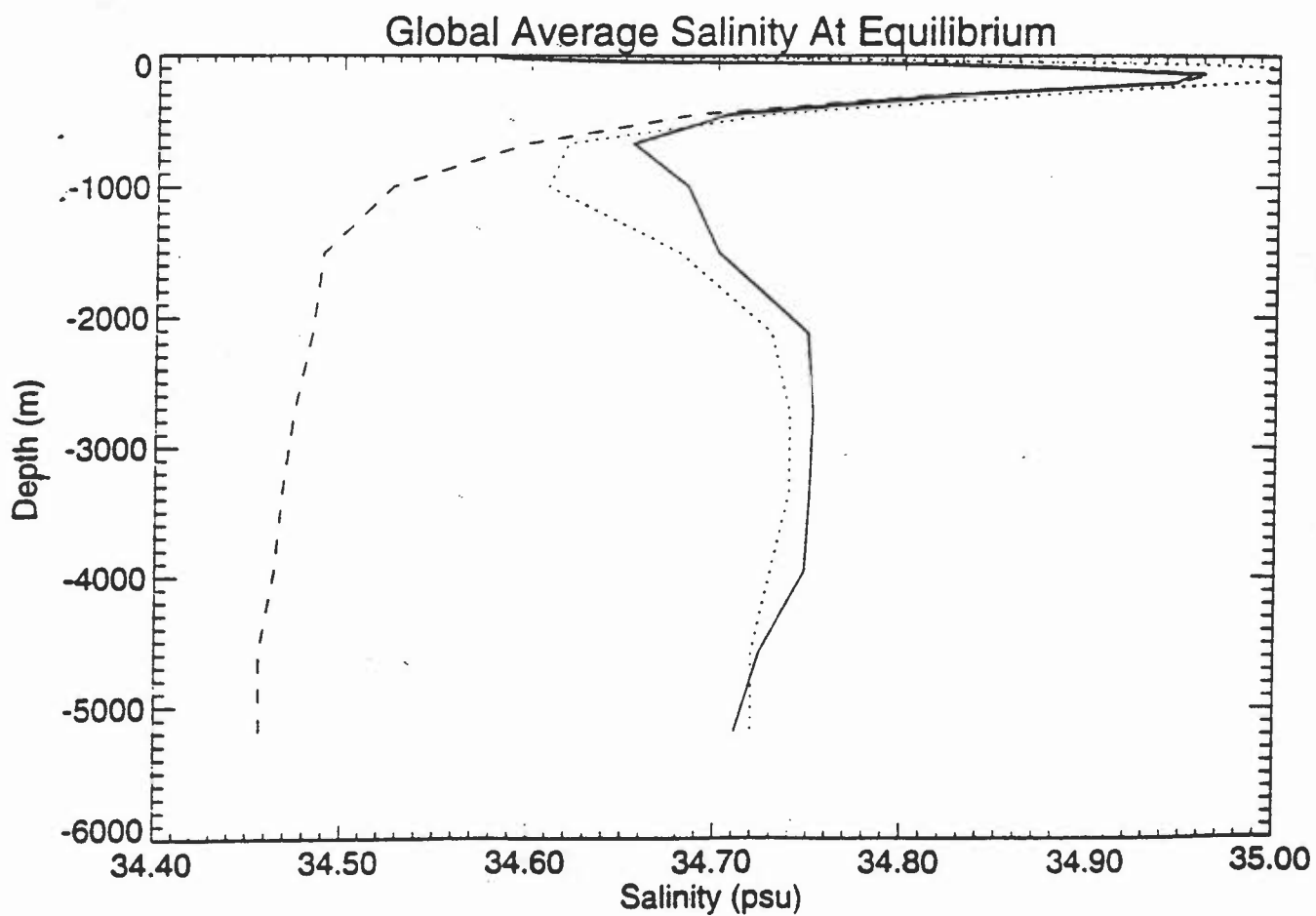
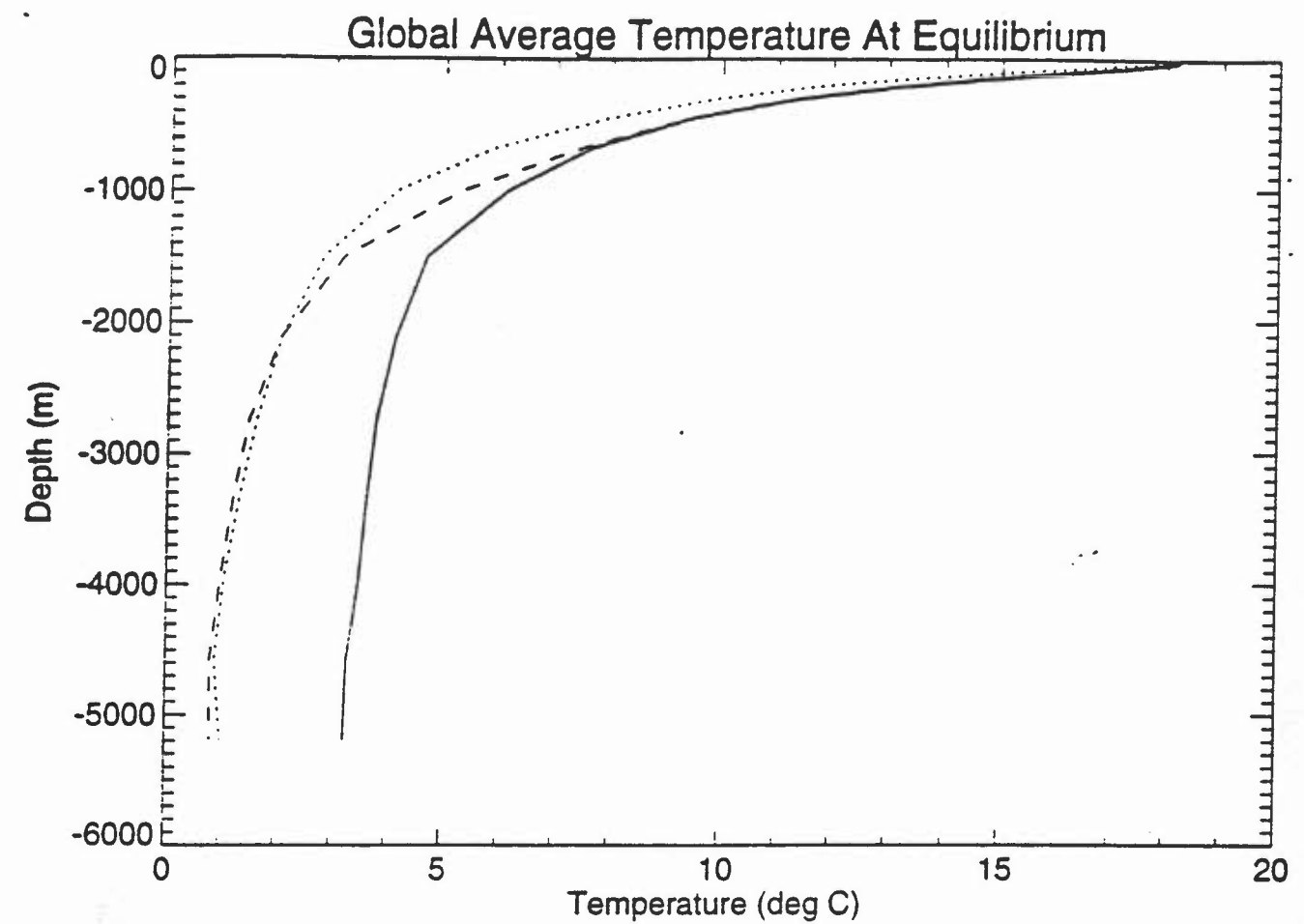


Figure 21. Profiles of globally averaged potential temperature (a), and salinity (b) from runs with (—) and without (---) the Mediterranean outflow parametrisation, and from the observed Levitus climatology (.....).

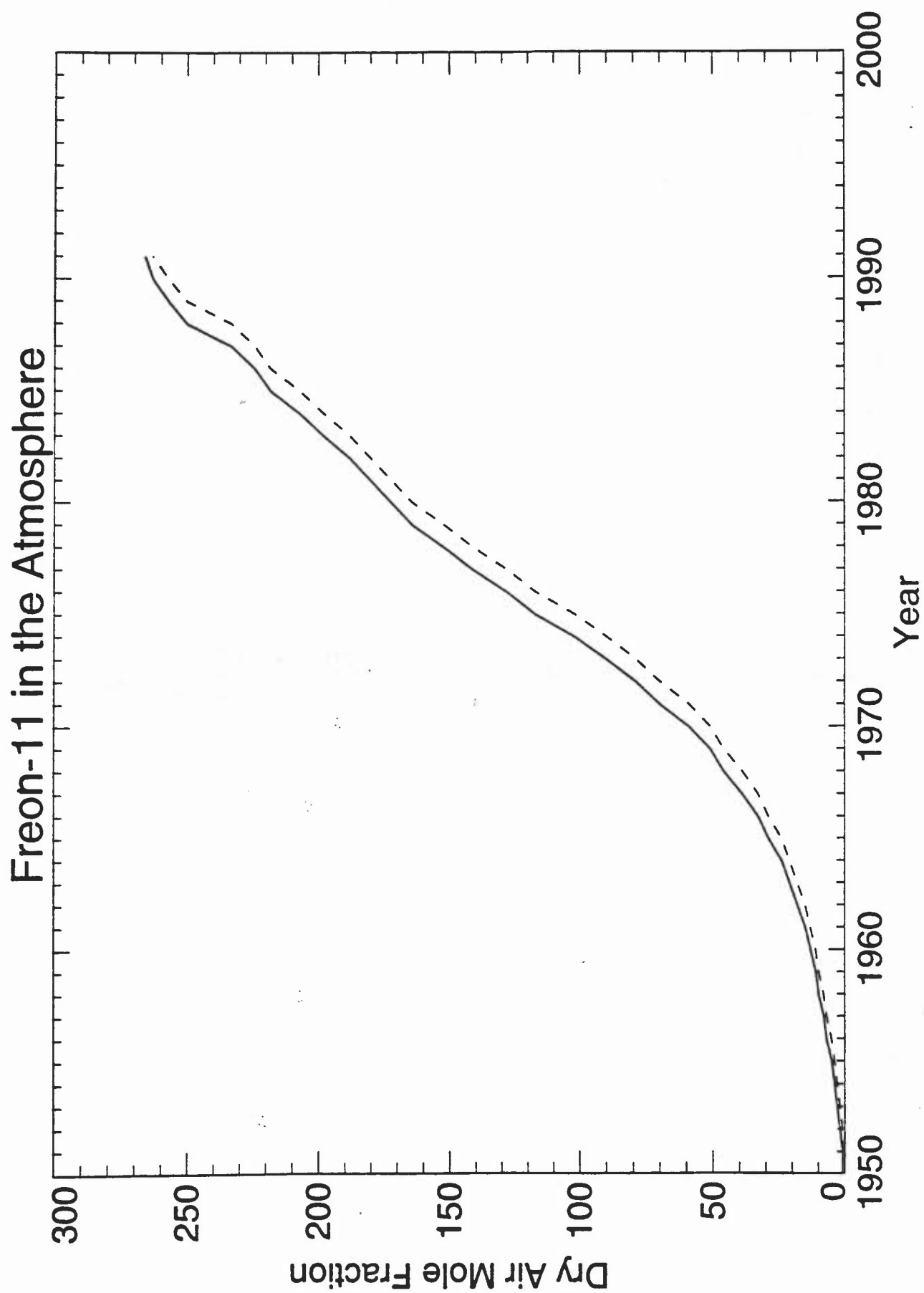


Figure 22. Time-history of the dry air mole fraction of CFC-11 in the atmosphere since 1950. This function was used as the atmospheric boundary condition for the simulation of CFC-11 uptake. The southern hemisphere history (----) lags the northern hemisphere history (—) slightly.

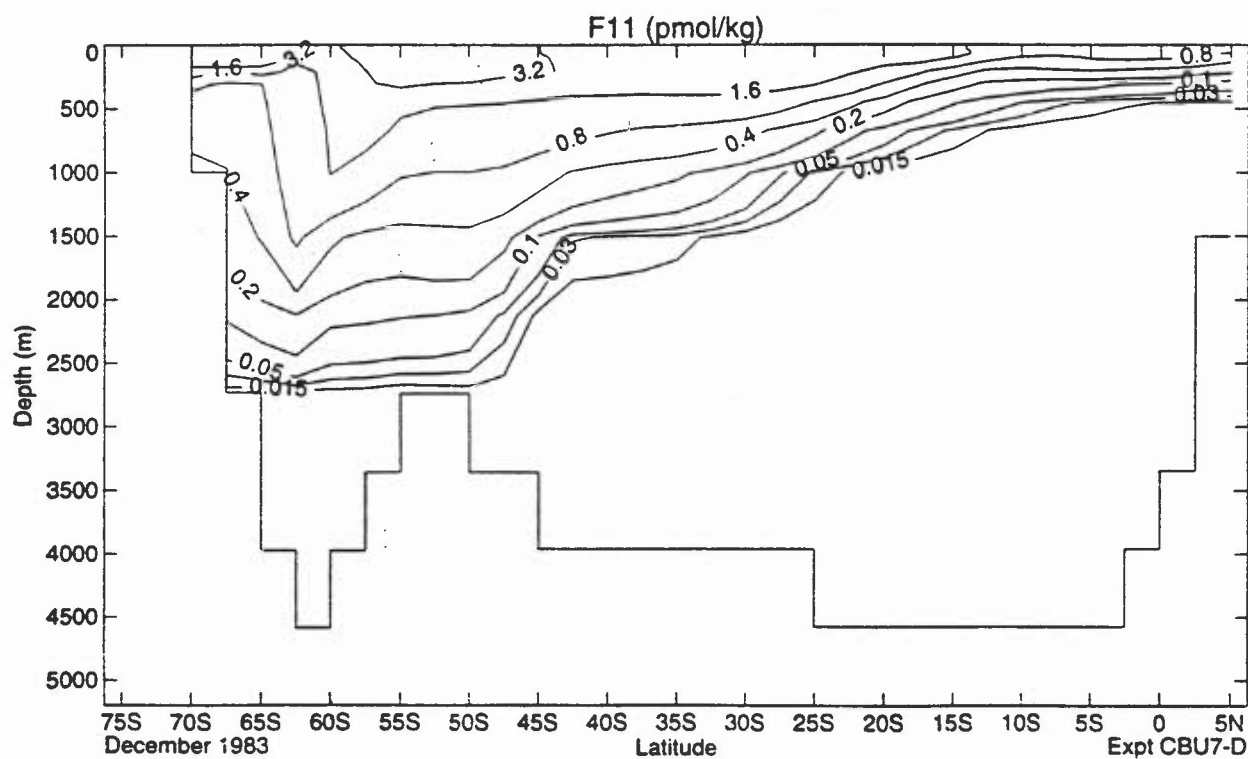
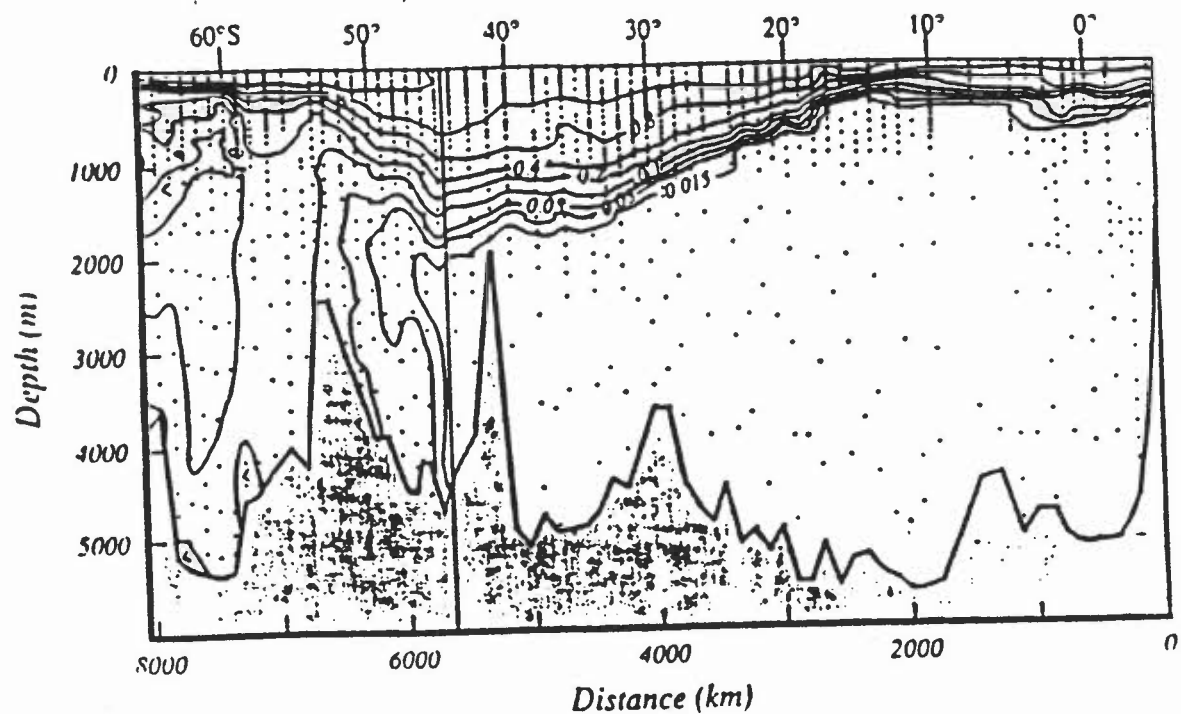


Figure 23. a) Observed distribution of CFC-11 along the Greenwich Meridian during late 1983 (from Warner and Weiss, 1992). b) Model distribution along the same section for December 1983. Contour levels are at 0.015, 0.03, 0.05, 0.1, 0.2, 0.4, 0.8, 1.6 and 3.2 pico-mol kg^{-1} .

